

## New Ultracool Companions to Nearby White Dwarfs

ALEXIA BRAVO ,<sup>1</sup> ADAM C. SCHNEIDER ,<sup>1</sup> SARAH CASEWELL ,<sup>2</sup> AUSTIN ROTHERMICHE ,<sup>3</sup>  
 JACQUELINE K. FAHERTY ,<sup>3</sup> JENNI R. FRENCH ,<sup>4</sup> THOMAS P. BICKLE ,<sup>5,6</sup> AARON M. MEISNER ,<sup>7</sup>  
 J. DAVY KIRKPATRICK ,<sup>8</sup> MARC J. KUCHNER ,<sup>9</sup> ADAM J. BURGASSER ,<sup>10</sup> FEDERICO MAROCCHI ,<sup>8</sup>  
 JOHN H. DEBES ,<sup>11</sup> ARTTU SAINIO ,<sup>6</sup> LÉOPOLD GRAMAIZE ,<sup>6</sup> FRANK KIWY ,<sup>6</sup> PETER A. JAŁOWICZOR ,<sup>6</sup> AND  
 AWAB ABDULLAHI 

<sup>1</sup>United States Naval Observatory, Flagstaff Station, 10391 West Naval Observatory Rd., Flagstaff, AZ 86005, USA

<sup>2</sup>School of Physics and Astronomy, University of Leicester, University Road, Leicester, LE1 7RH, UK

<sup>3</sup>Department of Astrophysics, American Museum of Natural History, Central Park West at 79th St., New York, NY 10024, USA

<sup>4</sup>School of Physics and Astronomy, University of Birmingham, Edgbaston, Birmingham, B15 2TT, UK

<sup>5</sup>School of Physical Sciences, The Open University, Milton Keynes, MK7 6AA, UK

<sup>6</sup>Backyard Worlds: Planet 9

<sup>7</sup>NSF's National Optical-Infrared Astronomy Research Laboratory, 950 N. Cherry Ave., Tucson, AZ 85719, USA

<sup>8</sup>IPAC, Mail Code 100-22, Caltech, 1200 E. California Blvd., Pasadena, CA 91125, USA

<sup>9</sup>Exoplanets and Stellar Astrophysics Laboratory, NASA Goddard Space Flight Center, 8800 Greenbelt Road, Greenbelt, MD 20771, USA

<sup>10</sup>Center for Astrophysics and Space Science, University of California San Diego, La Jolla, CA 92093, USA

<sup>11</sup>AURA for ESA, Space Telescope Science Institute, 3700 San Martin Drive, Baltimore, MD 21218, USA

## ABSTRACT

We conducted a search for new ultracool companions to nearby white dwarfs using multiple methods, including the analysis of colors and examination of images in both the optical and the infrared. Through this process, we identified fifty-one previously unrecognized systems with candidate ultracool companions. Thirty-one of these systems are resolved in at least one catalog, and all but six are confirmed as co-moving companions via common proper motion and consistent parallax measurements (when available). We have followed up four co-moving companions with near-infrared spectroscopy and confirm their ultracool nature. The remaining twenty candidates are unresolved, but show clear signs of infrared excess which is most likely due to the presence of a cold, low-mass companion or a dusty circumstellar disk. Three of these unresolved systems have existing optical spectra that clearly show the presence of a cool stellar companion to the white dwarf primary via spectral decomposition. These new discoveries, along with our age estimates for the primary white dwarfs, will serve as valuable benchmark systems for future characterization of ultracool dwarfs.

## 1. INTRODUCTION

The first L-dwarf (GD 165B) was discovered as a companion to a nearby white dwarf (Becklin & Zuckerman 1988). While thousands of L, T, and Y type dwarfs have been discovered since, the number of confirmed substellar companions to white dwarf primaries has remained relatively small. Other L, T, and Y type companions to white dwarfs include PHL 5038B (Steele et al. 2009), LSPM J1459+0857B (Day-Jones et al. 2011), WD 0806-661B (Luhman et al. 2011), Wolf 1130C (Mace et al. 2013), LSPM J0241+2553B (Deacon et al. 2014), LSPM J0055 + 5948AB (Meisner et al. 2020), COCONUTS-1B (Zhang et al. 2020), SDSS J222551.65+001637.7B (French et al. 2023), and VVV 1256–62AB (Zhang et al. 2024b). Several more candidates have also recently been

uncovered (e.g., Kiwy et al. 2022; Rothermich et al. 2024) and are awaiting spectroscopic confirmation.

Despite their relative rarity, each system containing a white dwarf with a resolved ultracool dwarf (spectral type later than  $\sim$ M7) companion holds great value as a benchmark system. It is typically very difficult to determine a precise age of a solitary ultracool dwarf, and often their distances are difficult to measure because of their inherent faintness. If a cool companion can be physically tied to a white dwarf primary, the age and distance of the white dwarf, which are often much easier to determine, can be applied to the cold secondary.

For objects with masses below the substellar limit (brown dwarfs), companionship can be especially valuable because brown dwarfs cool over time, resulting in a degenerate relationship between age, effective temperature ( $T_{\text{eff}}$ ), and mass. White dwarf primaries with

measurable ages can break this degeneracy leading to much more precise physical property determination for any brown dwarf companion (e.g., Luhman et al. 2011; Mace et al. 2018; Zhang et al. 2020). White dwarfs in particular have very predictable cooling rates, which is why they are often used to determine the ages of nearby stars (e.g., Fouesneau et al. 2019; Qiu et al. 2021; Baig et al. 2024), stellar clusters (e.g., Salaris & Bedin 2018; Lodieu et al. 2019a,b; Heyl et al. 2022), and larger populations (e.g., Kilic et al. 2019).

Additional low-mass companions to white dwarfs have been found through indirect means, such as radial velocity variations (e.g., Maxted et al. 2006; Casewell et al. 2012; Farihi et al. 2017), photometric transits (e.g., Beuermann et al. 2013; Parsons et al. 2017; Casewell et al. 2020b), or photometric/spectral decomposition (e.g., Farihi & Christopher 2004; Dobbie et al. 2005; Steele et al. 2011, 2013; Casewell et al. 2018, 2020a; Owens et al. 2023). These systems, however, are often products of post-common envelope evolution. While their utility as age benchmarks is not as clear as with wide ultracool companions, these systems provide rare laboratories for studying the effects of radiation on substellar atmospheres.

We have used the substantial increase in the number of known nearby (<100 pc) white dwarfs enabled by Gaia (Gaia Collaboration et al. 2021a) in Gentile Fusillo et al. (2021) to search for new ultracool companions in the solar neighborhood. We describe our candidate selection methods in Section 2, follow-up observations in Section 3, system properties in Section 4, an analysis of newly discovered systems in Section 5, and provide a conclusion in Section 6.

## 2. CANDIDATE SEARCH

### 2.1. *The White Dwarf Sample*

Our initial list of white dwarfs came from Gentile Fusillo et al. (2021) which is derived from the Gaia Early Data Release 3 (Gaia Collaboration et al. 2021a) catalog and contains  $\sim 1.3$  million likely white dwarfs. Our objective is to search for ultracool companions, which are inherently faint. We therefore limited our initial sample to white dwarfs within 100 pc ( $\varpi \geq 10$  mas). This distance requirement resulted in a candidate list of 16,959 objects.

We employed three different search methods with this sample in order to identify a comprehensive set of both unresolved and resolved candidate companions. These three methods included identifying color outliers, visually inspecting optical and infrared images of each white dwarf for cool companions, and finding ultracool candidates using Gaia astrometry and photometry. Each

method is described in detail in the following three sections.

#### 2.1.1. *Method I: Color Cuts*

This method involved identifying color-selected outliers within our sample of white dwarf candidates. We cross-matched each source with the nearest detection in the CatWISE2020 catalogue (Marocco et al. 2021). We propagate the positions of each candidate white dwarf to the CatWISE 2020 epoch ( $\sim 2015$ ) using Gaia proper motions and use a 5'' search radius. We use the proper motion corrected CatWISE 2020 photometry (e.g., w1mpro\_pm and w2mpro\_pm) for all sources. We also cross-matched each white dwarf with available near-infrared surveys using proper motion corrected coordinates, including the UKIRT Hemisphere Survey (UHS; Dye et al. 2018); the UKIRT Infrared Deep Sky Survey (UKIDSS) Large Area Survey (LAS; Lawrence et al. 2007), Galactic Plane Survey (GPS; Lucas et al. 2008), and Galactic Clusters Survey (GCS; Lawrence et al. 2007); the Visible and Infrared Survey Telescope for Astronomy Hemisphere Survey (VHS; McMahon et al. 2013), VISTA Variables in the Via Lactea (VVV; Minniti et al. 2010), VISTA Magellanic Clouds (VMC; Cioni et al. 2011), and VISTA Kilo-degree Infrared Galaxy (VIKING; Edge et al. 2013) surveys. We then created several color-color plots using Gaia, near-infrared, and CatWISE magnitudes.

Using a sample known white dwarf-brown dwarf systems from the literature (including both resolved and unresolved companions), we searched for color combinations that differentiated the known white dwarf-brown dwarf sample from the rest of the white dwarf population. We determined that the  $G_{\text{BP}} - G_{\text{RP}}$  vs.  $G - W2$  color color diagram clearly distinguished these two populations. The Gaia filters have pivot wavelengths of 621.79 nm, 510.97 nm, and 776.91 nm for  $G$ ,  $G_{\text{BP}}$ , and  $G_{\text{RP}}$ , respectively (Riello et al. 2018), while the WISE W2 filter has a reference wavelength of 4.6028  $\mu\text{m}$  (Wright et al. 2010). The non-excess white dwarfs show a clear correlation between  $G_{\text{BP}} - G_{\text{RP}}$  and  $G - W2$  colors, with redder  $G_{\text{BP}} - G_{\text{RP}}$  colors corresponding to redder  $G - W2$  colors. Both of these colors have been shown to correlate with absolute  $G$ -band magnitudes, with redder colors corresponding to fainter absolute magnitudes (e.g., Gaia Collaboration et al. 2018; Kirkpatrick et al. 2024). Thus this trend can generally be viewed as a temperature sequence, with the coldest white dwarfs having the reddest  $G_{\text{BP}} - G_{\text{RP}}$  and  $G - W2$  colors. We selected as candidates those objects with  $G_{\text{BP}} - G_{\text{RP}}$  colors less than  $0.417 \times (G - W2) - 0.10$  mag (see Figure 1), which cleanly selected a large sample of known, blended

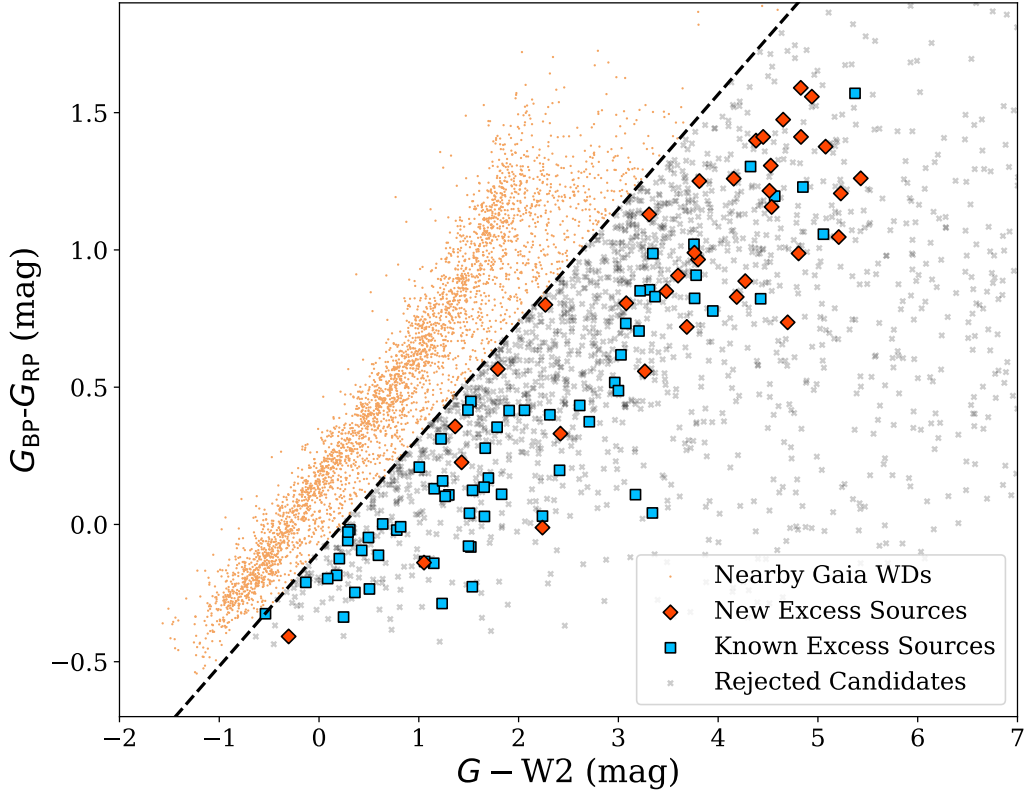


**Figure 1.**  $G_{\text{BP}} - G_{\text{RP}}$  vs.  $G - \text{W2}$  colors for Gaia white dwarfs within 100 pc from Gentile Fusillo et al. (2021). Objects on the normal white dwarf color sequence are displayed as orange dots. Objects showing signs of infrared excess were selected as having redder  $G - \text{W2}$  colors than the dashed line. The color positions of previously known excess sources and newly discovered excess candidates selected via Method I are shown as blue squares and red diamonds, respectively. Rejected excess candidates are shown with grey x symbols.

white dwarf/ultracool dwarf systems. However, this color selection criteria still suffered from significant contamination, mostly from blending with bright sources with small separations. We attempted to eliminate spurious candidates by first flagging those sources with another Gaia source within  $3''$ , thereby eliminating many white dwarf candidates that were blended with a nearby, bright Gaia source. We also required CatWISE2020 W2 magnitudes to have a signal-to-noise ratio (S/N) greater than 10.

These cuts resulted in a total of 3,095 candidates. Each of these candidates was then individually inspected using available optical and infrared images. The vast majority of these sources still showed clear signs of contamination, typically in the form of blending with an unrelated nearby source. The remaining sources, highlighted in Figure 1, either showed no clear contamination, or were found to have a resolved companion within a few arcseconds.

### 2.1.2. Method II: Visual Inspection

This method entailed the manual inspection of available optical images, such as those from the Panoramic Survey Telescope and Rapid Response System (Pan-STARRS (PS1); Chambers et al. 2016) and the Dark Energy Survey (DES; Abbott et al. 2021). For each of the 16,959 objects in our white dwarf sample, we inspected optical images (when available) to identify by-eye any sources within  $\sim 30''$  with exceptionally red optical colors. A search radius of  $30''$  was chosen because it is sufficiently large to expand the search area covered by Method I, but is also small enough to not be subject to an excessive amount of false positives. While this search recovered some of the same sources found using the method in Section 2.1.1 that were resolved in optical or near-infrared images, but not resolved in the Wide Field Infrared Survey Explorer (WISE; Wright et al. 2010) imagery, it was also sensitive to wider sep-

aration companions that would not easily be identified by colors of the white dwarf alone.

Red colors do not guarantee that a candidate companion is co-moving with the white dwarf primary. For those with Gaia parallaxes and proper motions, we ensured consistency between candidate companions and the nearby white dwarfs. For those candidate companions not in Gaia, we either used proper motions from relevant catalogs, such as CatWISE2020 or the NOIRLab Source Catalog DR2 (NSC; Nidever et al. 2021), or calculated proper motions from available catalog detections from UKIDSS, UHS, or PS1. For UHS and UKIDSS, positions were calibrated using the Gaia DR3 reference frame following Schneider et al. (2023). For PS1, detections were taken directly from the DR2 catalog. If detections existed in UKIRT and PS1 catalogs, they were not mixed to avoid systematics between catalogs. Time baselines were several years from each catalog, and thus parallactic motion should have a negligible effect on the resulting proper motions. We ensured that companion candidates had proper motions and parallax (when available) measurements that agreed to within  $5\sigma$ , or had proper motion measurements with differences less than  $5 \text{ mas yr}^{-1}$  and parallax measurement differences less than 1 mas. The second selection criteria was necessary for pairs with exceptionally small measurement uncertainties. For example, while the A and B components of the  $4''$  separation WD J1046+6054AB system have  $\mu_\alpha$  and  $\mu_\delta$  differences of only 3.2 and 2.7 mas  $\text{yr}^{-1}$ , respectively, their small uncertainties result in  $18\sigma$  and  $13\sigma$  disagreements.

There are two exceptions to the above requirements. The first is the companion candidate to WD J001237.06–492422.81, which initially had proper motion differences of less than  $2\sigma$  using the relatively imprecise proper motion measurement of the companion candidate from CatWISE 2020 (Marocco et al. 2021). A more precise proper motion measurement was later found in NSC DR2 (Nidever et al. 2021), resulting in larger discrepancies between  $\mu_\alpha$  ( $14\sigma$ ) and  $\mu_\delta$  ( $4\sigma$ ) components. While this object is still listed in Table 4, it is unlikely to be a physical pair. Second, the putative companion to WD J211901.60+420617.34 was observed spectroscopically before being fully vetted kinematically. We include it in Table 4 despite its unlikely physical nature. For a few candidates, we were unable to produce a proper motion precise enough to clearly establish companionship. We retain these sources for completeness, but label them as “unreliable” until more precise proper motions can be measured.

We also estimated spectral types for each candidate companion. The focus of this work is to identify new

companions with spectral types  $\sim\text{M7}$  and later. We used Gaia parallaxes of candidate companions when available, or the parallax of the putative white dwarf primaries, to calculate absolute  $G$ -,  $J$ - and  $K$ -band magnitudes. We compared these values to the absolute  $G$ -band magnitude versus spectral type table from Kiman et al. (2019), absolute  $J$ - and  $K$ -band values from Pecaut & Mamajek (2013), and the absolute  $J$ - and  $K$ -band versus spectral type relations from Schneider et al. (2023) to estimate spectral types for each companion. Estimated spectral types from different passbands generally agreed to within  $\pm 1$  subtype. In cases where the different relations resulted in different spectral type estimates, the median type was chosen. Candidates with estimated types of  $\sim\text{M7}$  and later were retained.

During the visual examination of optical images for objects from Gentile Fusillo et al. (2021), we identified two objects that appeared unlikely to be white dwarfs based on their red-optical colors (WD J224600.88–060947.02 and WD J235432.47+080404.64). WD J224600.88–060947.02 was previously identified by O’Brien et al. (2024) as a likely brown dwarf contaminant in the Gentile Fusillo et al. (2021) sample. We suggest WD J235432.47+080404.64 is also likely a low-mass star or brown dwarf. Using Gaia parallaxes and photometry from VHS for WD J224600.88–060947.02 and UKIDSS LAS for WD J235432.47+080404.64, we find absolute magnitude consistent with spectral types of  $\sim\text{L2}$  for WD J224600.88–060947.02 and  $\sim\text{L1}$  for WD J235432.47+080404.64.

### 2.1.3. Method III: Gaia Comparisons

Our final method of identifying potential ultracool companions used available Gaia astrometry and photometry for objects within the vicinity of each nearby white dwarf. We identified every object with Gaia distances  $<110$  pc within  $60''$  of each object in our white dwarf sample. We chose 110 pc to account for some uncertainty in both white dwarf and candidate companion parallax measurements. For each object within  $60''$  of one of our white dwarf targets that had a distance measurement within 110 pc, we individually checked for relative proper motion and parallax consistency, to be further evaluated with the CoMover tool (see Section 2.2.2). We further selected for possible ultracool companions by identifying those sources with absolute  $G$ -band magnitudes  $>14.5$  mag, which corresponds to a spectral type of  $\sim\text{M8}$ . We did not require any further color-cuts based on Gaia colors, as the redness of ultracool sources can make the Gaia photometry unreliable (Smart et al. 2019). However, we did note that

some white dwarfs were found to match to each other (i.e., white dwarf-white dwarf systems). These candidate systems are listed in Appendix A.

## 2.2. Final Candidates

### 2.2.1. Unresolved Candidates

Our unresolved candidates were found solely through Method I (Section 2.1.1). A total of seventy-four unresolved candidate systems were identified. We searched the literature for each candidate to determine if these objects were previously known to have infrared excess, which could be indicative of an unresolved companion or dusty debris disk. Fifty-seven of our unresolved candidates were determined to have been previously identified as having either a known debris disk, an unresolved companion, or general infrared excess. These sources are listed in Table 1. Seventeen of our unresolved candidates had not been previously reported. These objects are listed in Table 2 with their corresponding Gaia and CatWISE2020 photometric measurements. Optical and WISE images for each of these candidates is shown in Figure 2. The infrared excess of these white dwarfs could suggest the presence of a surrounding dust disk, or alternatively an unresolved low-mass companion (explored further in Section 5).

We note that the results of our search for white dwarfs showing signs of excess infrared emission are different from previous searches because of our specific color-selection criteria and the construction of our input sample. Because we are most interested in new, cold companions to white dwarfs, a distance-limited sample is most appropriate, as such companions are inherently faint. Other infrared-excess searches focused on white dwarfs (e.g., Favieres et al. 2024) instead use a magnitude limited sample, which would be sensitive to excess emission around bright white dwarfs beyond 100 pc that are not included in our sample.

**Table 1.** Previously Known IR Excess Systems

System	Ref
WD J004912.03+384130.49	1
WD J005045.82−032655.47	1
WD J005815.51−563810.16	2
WD J010726.22+251835.60	1
WD J010749.38+210745.84	1
WD J010933.16−190117.56	3
WD J011221.14−561427.51	4

**Table 1** *continued*

**Table 1** (*continued*)

System	Ref
WD J013326.41+040104.57	5
WD J013532.98+144555.90	6
WD J014754.82+233943.60	7
WD J020524.94−794103.78	1
WD J020733.81+333129.53	8
WD J021912.81−630654.86	9
WD J022320.55−045906.66	1
WD J023427.73−045430.68	10
WD J030253.10−010833.80	11
WD J033645.45+704411.16	1
WD J035817.13+462839.74	12
WD J040435.02+150226.60	13
WD J040911.40−711741.56	14
WD J041653.28+262420.41	15
WD J041937.77−730344.51	16
WD J043354.57+282729.07	1
WD J043839.37+410932.35	17
WD J051002.15+231541.42	1
WD J053112.43−245120.86	2
WD J054224.17+014414.64	18
WD J070245.87+000318.99	1
WD J075508.95−144550.95	21
WD J080227.74+563155.46	1
WD J081149.35+421208.95	18
WD J093341.31−100009.20	1
WD J094755.68−231234.10	13
WD J100609.17+004417.08	19
WD J101728.52−323608.84	1
WD J101803.83+155158.57	17
WD J105212.55+332318.39	1
WD J111424.68+334124.39	20
WD J111912.40+022033.05	17
WD J121314.48+114050.14	2
WD J122305.09−293228.29	3
WD J125224.22−291456.00	22
WD J130542.40+180103.77	23
WD J131246.44−232132.60	24
WD J142833.74+440346.94	1
WD J143830.09−312719.79	9
WD J145006.66+405535.20	16
WD J154144.89+645352.98	18
WD J160839.55+172336.67	25
WD J161316.63+552125.97	18
WD J165126.05+663506.34	26
WD J172349.68+045847.54	1
WD J172845.71+205341.68	1
WD J173134.32+370520.71	27

**Table 1** *continued*

**Table 1** (*continued*)

System	Ref
WD J190319.56+603552.65	1
WD J222958.08+302410.01	1
WD J225726.12+075542.60	25
WD J232847.64+051454.24	28
WD J233401.45+392140.87	2
WD J234036.64–370844.72	10

**References**—(1) Rebassa-Mansergas et al. (2019); (2) Favieres et al. (2024); (3) Dennihy et al. (2017); (4) Girven et al. (2012); (5) Ren et al. (2018); (6) Casewell et al. (2020a); (7) Wang et al. (2019); (8) Debes et al. (2019); (9) Raddi et al. (2017); (10) Thorstensen et al. (2016); (11) Casewell et al. (2020a); (12) Greenstein (1986); (13) Xu et al. (2020); (14) Kraft & Luyten (1965); (15) Ren et al. (2014); (16) Hoard et al. (2013); (17) Farihi et al. (2005); (18) Girven et al. (2011); (19) Schultz et al. (1996); (20) Raymond et al. (2003); (21) Rebassa-Mansergas et al. (2010); (22) Mumford (1969); (23) Nather et al. (1981); (24) Ruiz et al. (2001); (25) Debes et al. (2011); (26) Lai et al. (2021); (27) Kilic et al. (2005); (28) Zuckerman & Becklin (1987); (29) Rodríguez-Gil et al. (2005)

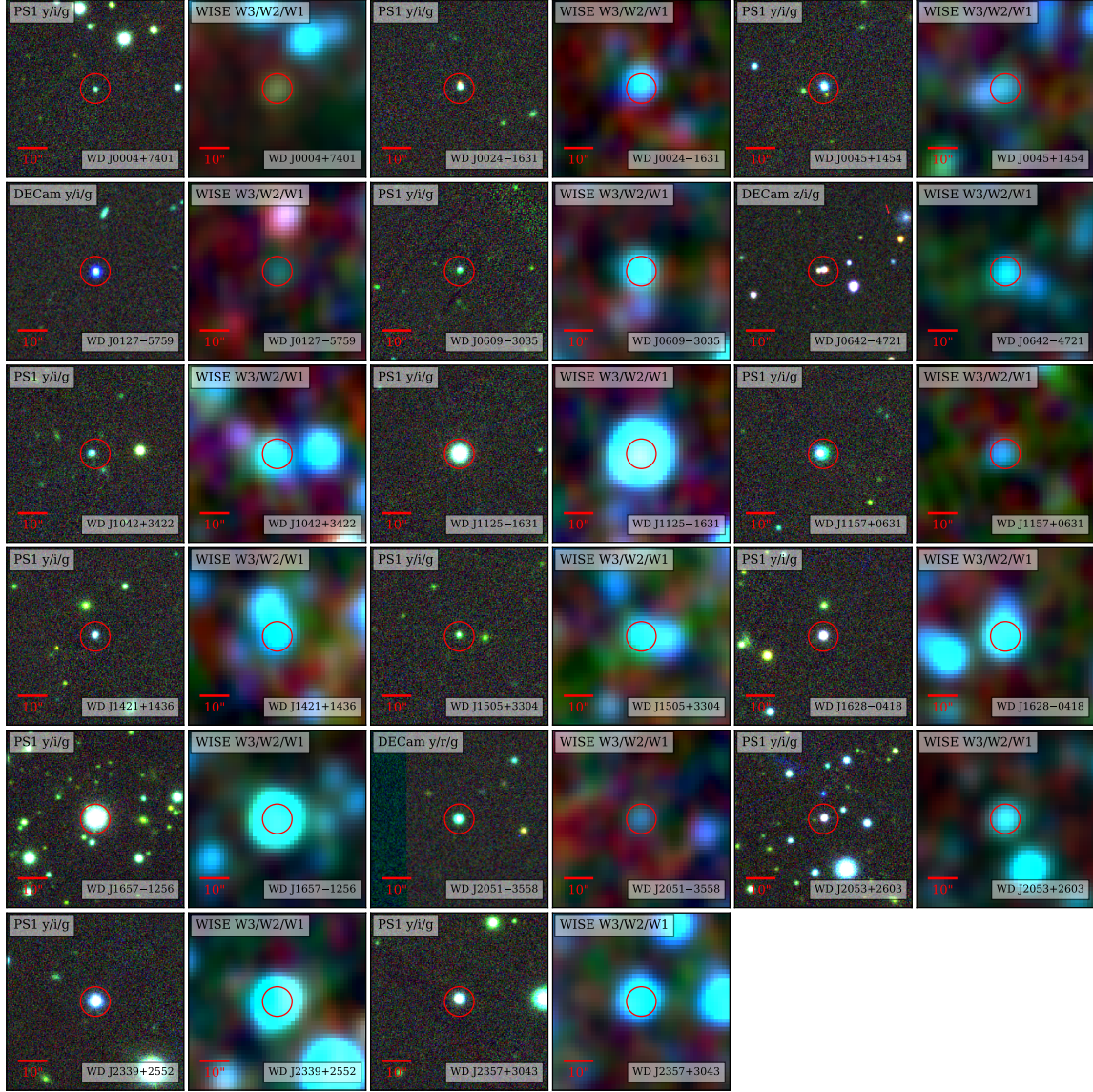


**Figure 2.** Three color RGB optical and WISE images of all new unresolved candidates. Optical images either come from Pan-STARRS (PS1; Chambers et al. 2016) or DECam images obtained through the Astro Data Lab image cutout service (Fitzpatrick et al. 2014; Nikutta et al. 2020). WD identifiers are listed for each object.

**Table 2.** Unresolved Candidates

WD Name	$\varpi$ (mas)	$\mu_\alpha$ (mas yr $^{-1}$ )	$\mu_\delta$ (mas yr $^{-1}$ )	$G$ (mag)	$G_{\text{BP}}$ (mag)	$G_{\text{RP}}$ (mag)	W1 (mag)	W2 (mag)
WD J00427.01+740141.77	10.8108±0.4736	25.751±0.600	92.855±0.587	20.2099±0.0060	20.7608±0.0843	19.3846±0.0558	16.214±0.025	15.133±0.025
WD J002455.00−163113.24	12.7572±0.3538	91.026±0.383	-73.071±0.291	19.4282±0.0039	20.0190±0.0542	18.7119±0.0300	15.199±0.020	14.901±0.027
WD J004558.03+145449.80	15.3367±0.1207	-9.667±0.159	-140.873±0.094	18.0909±0.0030	18.2887±0.0115	17.7224±0.0159	16.492±0.036	16.299±0.088
WD J012709.06−575914.45	10.5455±0.0691	-125.975±0.074	-100.091±0.074	17.7421±0.0030	17.7279±0.0100	17.8669±0.0136	17.577±0.062	16.690±0.092
WD J060942.14−303552.74	13.8173±0.2077	26.909±0.218	-151.904±0.251	19.2061±0.0037	19.6818±0.0413	18.4664±0.0269	14.936±0.017	14.692±0.021
WD J064244.74−472110.25	11.7956±0.3079	-29.702±0.326	162.089±0.371	19.8052±0.0052	20.1959±0.0865	18.7842±0.0513	15.219±0.020	14.975±0.021
WD J104203.04+342227.34	12.7616±0.3765	-289.601±0.414	-49.101±0.401	19.8001±0.0043	20.2390±0.0602	19.2517±0.0414	15.504±0.019	14.994±0.027
WD J112542.43−163154.24	21.5638±0.0429	11.886±0.048	-2.11±0.037	15.8768±0.0028	16.1853±0.0036	15.2789±0.0042	12.495±0.012	12.279±0.009
WD J115745.93+063148.28	13.0494±0.0877	-270.468±0.101	-24.079±0.065	17.2563±0.0029	17.3923±0.0067	17.0351±0.0081	16.308±0.034	15.892±0.064
WD J142152.24+143646.09	10.4251±0.2389	14.538±0.270	-68.285±0.210	18.9430±0.0037	19.3551±0.0381	18.3900±0.0285	15.322±0.019	15.144±0.032
WD J150549.34+330410.82	10.0124±0.4198	-22.958±0.299	-100.046±0.414	20.1376±0.0048	20.7498±0.0775	19.3516±0.0493	16.120±0.024	15.758±0.041
WD J162816.20−041810.26	11.0206±0.1284	-55.89±0.135	-40.297±0.101	17.9737±0.0030	18.4794±0.0147	17.2198±0.0108	13.957±0.015	13.818±0.015
WD J165737.30−125634.46	11.0374±0.0383	6.688±0.041	-10.134±0.031	15.0652±0.0029	15.3129±0.0033	14.5071±0.0044	12.178±0.013	11.986±0.009
WD J205148.28−355820.33	11.9003±0.1023	23.587±0.089	-16.476±0.079	17.4747±0.0029	17.5565±0.0082	17.3303±0.0098	16.699±0.043	16.046±0.071
WD J205357.06+260326.29	10.2420±0.1493	15.049±0.140	-23.11±0.138	18.5542±0.0031	19.1209±0.0279	17.7092±0.0135	14.286±0.014	14.103±0.015
WD J233910.91+255205.81	11.1455±0.0623	12.292±0.054	-32.474±0.044	16.5273±0.0029	16.6828±0.0053	16.1250±0.0053	13.481±0.012	13.262±0.011
WD J235745.75+304357.77	13.8718±0.5094	5.298±0.449	-203.983±0.330	17.7454±0.0041	17.8467±0.0100	16.8568±0.0068	14.199±0.013	13.983±0.014

NOTE—All positions and optical photometry come from Gaia (Gaia Collaboration et al. 2021a) and mid-infrared photometry comes from CatWISE 2020 (Marocco et al. 2021).

**Table 3.** Known Resolved Systems

System	Ref
WD J000801.26–350449.62ABC	1
WD J000837.22+351144.52AB	2
WD J013608.94–255614.10AB	2
WD J015501.26–130749.19AB	2
WD J024149.28+255344.60AB	3
WD J035556.50+452510.26AB	4
WD J052933.35–635655.29AB	5
WD J064111.04–202743.83AB	6
WD J082545.09–021024.73AB	2
WD J095953.92–502717.75AB	7
WD J120815.61+084543.16AB	8
WD J123304.35+030245.83AB	9
WD J124428.57–011857.85AB	9
WD J125646.05–620208.54AB	10
WD J131730.86+483333.05AB	11
WD J155516.93+315306.96AB	12
WD J162324.07+343647.37AB	13
WD J164119.19+350425.08AB	14
WD J184014.71+343846.50AB	15
WD J185520.08–231440.90AB	2
WD J192409.62+550648.48AB	15
WD J221536.67+134711.17AB	7
WD J234507.33+581315.07AB	16

**References**—(1) Tokovinin (2022); (2) Casewell et al. (in prep.); (3) Deacon et al. (2014); (4) Zhang et al. (2020); (5) Ravinet et al. (2024); (6) Girven et al. (2011); (7) Gaia Collaboration et al. (2021b); (8) Zhang et al. (2010); (9) Kiman et al. (2019); (10) Zhang et al. (2024b); (11) Jalowiczor et al. (2021); (12) Kiman et al. (2021); (13) Silvestri et al. (2006); (14) Silvestri et al. (2007); (15) Lépine & Shara (2005); (16) Rebassa-Mansergas et al. (2019)

### 2.2.2. Resolved Candidates

A combined total of 54 candidate white dwarf + ultracool dwarf systems that were resolved in at least one cat-

alog were identified using Methods I, II, III. A literature search revealed that 23 of these systems had been discovered previously. These recovered systems are listed in Table 3.

We found a total of 31 new systems with white dwarf primaries and candidate ultracool dwarf companions where the companions were resolved in at least one survey. Astrometric and photometric information are provided in Tables 4, 5, and 6. Available absolute magnitudes and spectral type estimates are given in Table 7. Cutout optical images of the candidate systems are shown in Figure 3. Note that the “unreliable” candidates are not included in Figure 3. All candidate systems were evaluated with the `CoMover` comoving probability tool, which determines the Bayesian probability of two sources being a physically comoving pair. `CoMover` probabilities are provided in Table 4.

Several of these resolved candidate companions had been noted as candidate ultracool dwarfs or high-proper motion objects in previous surveys, but had not been recognized as having a white dwarf companion. WD J014953.55–612916.97B, WD J023020.88–344749.38B, WD J044713.58–582318.04B, WD J104627.91+605448.32B, and WD J211901.60+420617.34B were each selected as Gaia ultracool dwarf candidates in Reylé (2018). WD J044713.58–582318.04B was also previously identified as a high proper motion source in Deacon & Hambly (2007) and Kirkpatrick et al. (2016). WD J104627.91+605448.32B has an optical spectral type of M9 in Kiman et al. (2019). WD J080648.05+221551.65B was selected as an L-type candidate object in Gálvez-Ortiz et al. (2017). Lastly, WD J141835.29+092919.68B was previously identified as a photometric L dwarf candidate in Skrzypek et al. (2016).

Several of these sources have also been identified as ultracool dwarf candidates by citizen scientists working with the Backyard Worlds: Planet 9 project (Kuchner et al. 2017). We recognize the contributions of these scientists in the footnotes of Table 4.

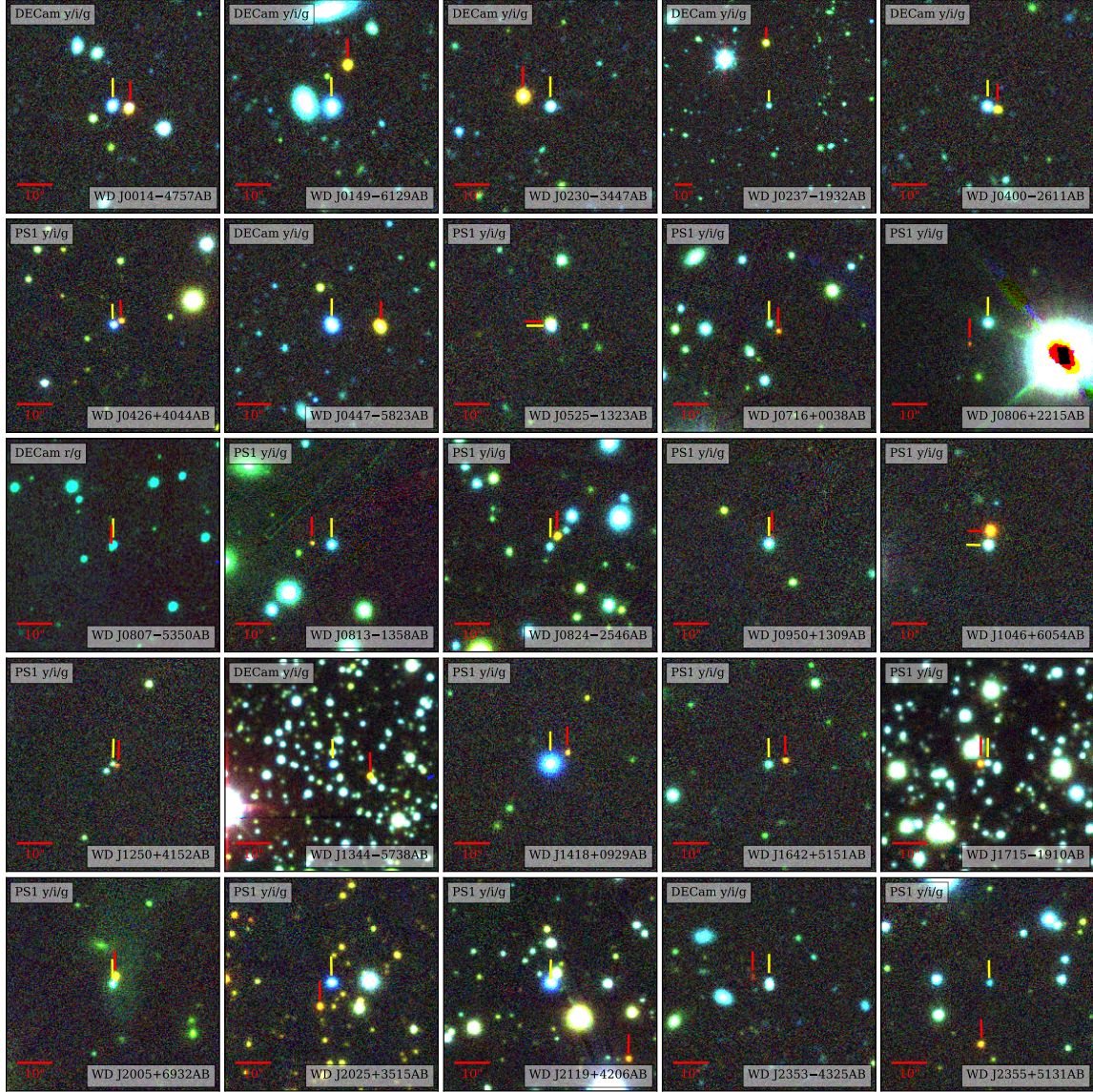


**Figure 3.** Three color RGB images of all new resolved candidates. White dwarf primaries are marked with yellow lines while candidate ultracool companions are marked with red lines. The WD 0807-5350 system has only  $r$ - and  $g$ -band DECam images, and thus the candidate companion is difficult to see in the image (though is resolved in Gaia). Note that the “unreliable” candidates are not included in this figure.

**Table 4.** Astrometry for Resolved Candidates

WD Name	R.A. ( $^{\circ}$ )	Dec. ( $^{\circ}$ )	Sep. ( $''$ )	$\varpi$ (mas)	$\mu_{\alpha}$ (mas yr $^{-1}$ )	$\mu_{\delta}$ (mas yr $^{-1}$ )	$\mu$ Ref.	CoMover (%)
WD J001237.06–492422.81 <sup>f</sup>	3.15476907	-49.40629603	10.4021±0.4282	52.587±0.256	9.574±0.373	1		
	3.15880278	-49.39958292	25.949	...	27.378±1.757	3.111±1.735	6	0.0
WD J001419.17–475719.58 <sup>a</sup>	3.58049053	-47.95620526	11.0341±0.1946	94.839±0.083	-172.360±0.147	1		
	3.57585816	-47.95643084	4.656	11.7522±0.7092	94.336±0.315	-175.836±0.606	1	100.0
WD J014953.55–612916.97	27.47317349	-61.48876565	13.0666±0.0544	3.697±0.060	-161.535±0.063	1		
	27.47050387	-61.48558188	12.316	13.1958±0.6313	5.231±0.721	-161.853±0.900	1	100.0
WD J023020.88–344749.38 <sup>b</sup>	37.58748692	-34.79751953	13.5645±0.2254	88.835±0.140	-106.153±0.212	1		
	37.59010968	-34.79674285	8.242	13.8045±0.2157	88.687±0.126	-106.918±0.199	1	100.0
WD J023703.94–193253.64	39.26657798	-19.545812689	12.8769±0.2640	35.157±0.262	24.646±0.269	1		
	39.26705588	-19.53837468	35.145	13.4481±0.1809	34.478±0.179	24.248±0.185	1	100.0
WD J032438.66+602055.88 <sup>f</sup>	51.16129325	60.34885745	14.905±0.0413	22.585±0.044	0.794±0.045	1		
	51.16544189	60.34854642	7.554	...	-14.04±8.160	2.900±8.160	4	57.4
WD J035637.43+321205.01 <sup>f</sup>	59.15615247	32.20120185	10.8855±0.1823	40.655±0.219	-42.978±0.160	1		
	59.15685548	32.20250415	5.078	...	-13.810±0.840	-25.720±0.840	4	1.5
WD J040046.84–261127.88 <sup>bc</sup>	60.19489510	-26.19155300	10.1351±0.2233	-53.982±0.142	-105.948±0.237	1		
	60.19402800	-26.19183500	2.594	...	-55.980±6.250	-102.780±6.280	4	100.0
WD J042641.33+404441.95	66.67226689	40.74489314	11.2170±0.1776	8.511±0.206	-21.259±0.163	1		
	66.67143120	40.74522229	2.556	...	21.290±4.380	-23.970±4.280	4	99.7
WD J044713.58–582318.04 <sup>d</sup>	71.80782392	-58.38735132	11.9753±0.0804	144.688±0.106	223.410±0.112	1		
	71.80068429	-58.38746020	13.478	11.8855±0.2510	143.481±0.324	222.571±0.356	1	100.0
WD J05255.93–132306.14	81.48317336	-13.38457114	12.7147±0.1510	25.155±0.137	105.459±0.148	1		
	81.48324826	-13.38423666	1.232	12.8550±0.3505	20.137±0.439	103.773±0.379	1	100.0
WD J063247.36+562851.61 <sup>f</sup>	103.19740550	56.48103159	10.1117±0.3520	10.907±0.245	6.823±0.200	1		
	103.19782560	56.48043620	2.460	...	9.260±7.360	29.000±7.360	2	99.6
WD J071609.53+003845.42	109.03985530	0.64555161	10.0449±0.5858	28.578±0.543	-90.304±0.491	1		
	109.039150	0.644984	3.358	...	31.280±3.600	-100.750±3.500	2	99.9
WD J073504.07–794410.69 <sup>f</sup>	113.76710360	-79.73633667	10.3760±0.0434	5.641±0.058	-7.907±0.060	1		
	113.76953590	-79.73515280	4.640	...	37.750±46.100	23.610±42.700	3	99.0
WD J080648.05+221551.65 <sup>bc</sup>	121.70014940	22.26354315	20.2306±0.1295	-11.125±0.126	-181.042±0.080	1		
	121.70170060	22.26234460	7.787	...	-18.300±11.340	-183.470±12.060	1	99.9
WD J080700.06–535049.78	121.74985732	-53.84710492	13.9069±0.2493	-50.375±0.268	11.883±0.317	1		

**Table 4** *continued*

**Table 4** (*continued*)

WD Name	R.A. ( $^{\circ}$ )	Dec. ( $^{\circ}$ )	Sep. ( $''$ )	$\varpi$ (mas)	$\mu_{\alpha}$ (mas yr $^{-1}$ )	$\mu_{\delta}$ (mas yr $^{-1}$ )	$\mu$ Ref.	CoMover (%)
WD J081319.85–135825.24 <sup>d</sup>	121.75008980	-53.84741704	1.227	13.7964±1.0883	-44.250±1.195	15.130±1.491	1	100.0
WD J082459.63–254652.79 <sup>b</sup>	123.3320600	-13.97363171	13.0609±0.1494	-26.206±0.151	10.691±0.157	1		
WD J095004.78+130937.82	123.33419840	-13.97350404	5.582	...	-35.280±4.290	9.440±4.290	4	99.8
WD J104627.91+605448.32	126.24805090	-25.78062645	10.6518±0.3647	-86.185±0.282	157.933±0.262	1		
WD J123405.10+442750.07 <sup>†</sup>	126.24738718	-25.77977101	3.757	9.9408±0.6354	-84.208±0.450	157.595±0.444	1	100.0
WD J125044.44+415259.50	147.51965482	13.16008135	17.7597±0.1563	-55.338±0.187	-95.202±0.225	1		
WD J141835.29+092919.68 <sup>b</sup>	147.51945820	13.16069700	2.078	...	-40.830±27.200	-126.450±29.000	3	99.9
WD J164220.31+515150.98 <sup>a</sup>	161.61635690	60.91362902	21.6187±0.0972	8.503±0.078	46.585±0.088	1		
WD J171508.30–191029.62 <sup>d</sup>	161.61606317	60.91473344	4.009	21.5812±0.2066	5.318±0.157	43.842±0.193	1	100.0
WD J200550.39+693227.22 <sup>f</sup>	188.52092740	44.46374053	10.1323±0.3345	-48.873±0.198	-37.172±0.260	1		
WD J202533.25+351510.15 <sup>b</sup>	188.51936360	44.46728250	13.286	...	-29.450±8.330	-5.660±8.430	2	14.8
WD J211901.60+420617.34 <sup>†</sup>	192.6844836	41.8831214	1.229	...	-79.470±7.430	7.990±7.700	2	98.2
WD J235521.59+513106.10	206.09217325	-57.64030013	11.3164±0.1938	-102.910±0.159	-30.165±0.180	1		
WD J235319.73–432517.86 <sup>g</sup>	206.08682414	-57.64129857	10.915	11.7255±0.4434	-103.885±0.378	-31.290±0.400	1	100.0
WD J235521.59+513106.10	214.64091690	9.48868440	11.5405±0.0449	-29.125±0.056	-26.022±0.047	1		
WD J235521.59+513106.10	214.645675	9.489645	5.604	...	-29.420±4.980	-25.070±5.510	5	100.0
WD J235521.59+513106.10	250.58431770	51.86411101	10.1741±0.3777	-39.625±0.478	-12.588±0.474	1		
WD J235521.59+513106.10	250.58220948	51.86437633	4.783	...	-40.910±3.970	-11.710±3.960	4	100.0
WD J235521.59+513106.10	258.78452710	-19.17520009	15.7889±0.2672	-11.735±0.334	-68.499±0.226	1		
WD J235521.59+513106.10	258.78511871	-19.17524133	2.017	15.7888±0.4579	-10.815±0.582	-64.733±0.399	1	100.0
WD J235521.59+513106.10	301.45962820	69.54122246	14.9830±0.1668	-25.056±0.234	74.422±0.205	1		
WD J235521.59+513106.10	301.45890459	69.54182851	2.364	14.6706±0.2874	-22.079±0.396	73.001±0.372	1	100.0
WD J235521.59+513106.10	306.38844874	35.25250972	10.9730±0.0746	-18.947±0.071	-69.407±0.082	1		
WD J235521.59+513106.10	306.38957885	35.2525067367	7.398	10.8499±0.4254	-18.576±0.373	-70.040±0.462	1	100.0
WD J235521.59+513106.10	319.75682370	42.10456425	10.1232±0.0392	28.294±0.043	-56.703±0.041	1		
WD J235521.59+513106.10	319.74845991	42.09883801	30.398	11.6371±0.5564	21.572±0.599	-20.867±0.576	1	0.0
WD J235521.59+513106.10	358.33200230	-43.42287846	14.1042±0.5174	-34.803±0.470	-283.899±0.433	1		
WD J235521.59+513106.10	358.33375000	-43.42238880	4.955	...	-36.970±16.680	-282.050±16.650	6	100.0
WD J235521.59+513106.10	358.84052670	51.51811023	10.5125±0.3091	81.313±0.270	-56.934±0.272	1		
WD J235521.59+513106.10	358.84174019	51.51336131	17.311	10.7942±0.7163	82.521±0.609	-56.367±0.761	1	100.0

**Table 4** *continued*

**Table 4** (*continued*)

WD Name	R.A. ( $^{\circ}$ )	Dec. ( $^{\circ}$ )	Sep. ( $''$ )	$\varpi$ (mas)	$\mu_{\alpha}$ (mas yr $^{-1}$ )	$\mu_{\delta}$ (mas yr $^{-1}$ )	$\mu$ Ref.	CoMover (%)
---------	------------------------	------------------------	------------------	-------------------	-------------------------------------	-------------------------------------	------------	----------------

$\dagger$  Proper motions for these sources are not precise enough to firmly rule out or confirm physical association.  
 $\ddagger$  These systems are unlikely to be physical pairs. The possible companion to WD J211901.60+420617.34 was followed-up spectroscopically (Section 3), despite its low CoMover probability.

*a* Identified by Backyard Worlds citizen scientist Léopold Gramaize.

*b* Identified by Backyard Worlds citizen scientist Frank Kiwy.

*c* Identified by Backyard Worlds citizen scientist Tom Bickle.

*d* Identified by Backyard Worlds citizen scientist Awab Abdillahi.

*e* Identified by Backyard Worlds citizen scientist Christopher Tanner.

*f* Identified by Backyard Worlds citizen scientist Arittu Sainio.

*g* Identified by Backyard Worlds citizen scientist Austin Rothemich.

**References**—(1) Gaia DR3 (Gaia Collaboration et al. 2021a); (2) UHS (Dye et al. 2018; Schneider et al. 2023); (3) CatWISE 2020 (Marocco et al. 2021); (4) Pan-STARRS DR1 (Chambers et al. 2016), This work; (5) UKIDSS LAS (Lawrence et al. 2007), This work; (6) NSC DR2 (Nidever et al. 2021)

**Table 5.** Optical Photometry for Resolved Companions

WD Name	<i>G</i>	<i>G<sub>BP</sub></i>	<i>G<sub>RP</sub></i>	<i>g</i>	<i>r</i>	<i>i</i>	<i>z</i>	<i>y</i>	Optical Source	
	(mag)	(mag)	(mag)	(mag)	(mag)	(mag)	(mag)	(mag)		
WD J0012−4924B	21.1058 ± 0.0119	21.4001 ± 0.1770	19.7325 ± 0.1052	24.0977 ± 0.1465	22.3258 ± 0.0494	20.1014 ± 0.0130	19.1525 ± 0.0081	18.9283 ± 0.0173	1	
WD J0014−4757B	20.3254 ± 0.0050	21.7254 ± 0.1284	18.8303 ± 0.0226	21.2674 ± 0.0123	21.8619 ± 0.0287	19.1716 ± 0.0041	17.9558 ± 0.0026	17.5150 ± 0.0054	1	
WD J0149−6129B	20.5739 ± 0.0071	20.8254 ± 0.4157	19.1726 ± 0.0676	25.1062 ± 0.4038	22.2604 ± 0.0402	19.6117 ± 0.0064	18.1167 ± 0.0031	17.6817 ± 0.0062	1	
WD J0230−3447B	18.9590 ± 0.0033	21.3322 ± 0.0995	17.4195 ± 0.0088	22.3405 ± 0.0317	20.5743 ± 0.0083	17.9188 ± 0.0014	16.7030 ± 0.0009	16.3236 ± 0.0023	1	
WD J0237−1932B	18.7291 ± 0.0034	21.0786 ± 0.1415	17.2676 ± 0.0113	21.8223 ± 0.0836	20.5056 ± 0.0298	18.0492 ± 0.0068	16.9093 ± 0.0042	16.2883 ± 0.0045	2	
WD J0324+6020B	...	...	...	...	...	...	...	...	2	
WD J0356+3212B	...	...	...	...	...	21.0822 ± 0.0690	19.6702 ± 0.0238	18.6915 ± 0.0230	2	
WD J0400−2611B	...	...	...	...	...	21.6415 ± 0.0727	20.5789 ± 0.0774	19.7736 ± 0.0351	2	
WD J0426+4044B	...	...	...	...	23.6926 ± 0.0885	22.4834 ± 0.0381	20.3585 ± 0.0108	18.8640 ± 0.0053	1	
WD J0447−5823B	19.2811 ± 0.0044	21.0895 ± 0.1391	17.7795 ± 0.0142	>23.5590	21.3570	20.5831 ± 0.0890	19.1689 ± 0.0115	18.2433 ± 0.0273	2	
WD J0525−1323B	19.2593 ± 0.0041	...	...	22.9239 ± 0.0616	20.9196 ± 0.0125	18.2390 ± 0.0023	17.9098 ± 0.0014	16.7726 ± 0.0034	1	
WD J0653+5628B	...	...	...	23.2540 ± 0.0784	20.8534 ± 0.0174	18.1790 ± 0.0016	17.0438 ± 0.0015	...	3	
WD J0716+0038B	...	...	...	>24.7740	>22.3570	>20.8190	19.7758 ± 0.0438	18.7978 ± 0.0234	2	
WD J0735−7944B	...	...	...	>23.1870	>21.1490	20.9548 ± 0.0415	19.4493 ± 0.0301	18.4756 ± 0.0270	2	
WD J0806+2215B	...	...	...	25.6991 ± 0.3062	23.8785 ± 0.0915	21.5762 ± 0.0172	20.5244 ± 0.0218	...	3	
WD J0807−5350B	20.6217 ± 0.0111	...	...	...	...	21.5088 ± 0.0695	20.0639 ± 0.0172	18.9666 ± 0.0199	2	
WD J0813−1358B	...	...	...	>22.5200	>20.7150	21.0905 ± 0.0592	19.7224 ± 0.0296	18.7183 ± 0.0210	2	
WD J0824−2546B	20.1222 ± 0.0066	20.8530 ± 0.1260	18.6103 ± 0.0302	...	...	19.5073 ± 0.0111	18.1973 ± 0.0217	17.5394 ± 0.0068	2	
WD J0950+1309B	...	...	...	...	...	23.9706 ± 0.3467	20.8270 ± 0.0288	...	3	
WD J1046+6054B	18.9159 ± 0.0034	21.3125 ± 0.1416	17.3298 ± 0.0091	>20.1350	21.1886 ± 0.0560	18.3831 ± 0.0060	16.9785 ± 0.0069	16.1171 ± 0.0091	2	
WD J1234+4427B	...	...	...	...	...	20.4664 ± 0.0329	19.6619 ± 0.0203	19.1481 ± 0.0215	2	
WD J1250+4152B	...	...	...	...	21.0860 ± 0.2588	...	20.7318 ± 0.0861	19.5414 ± 0.0450	2	
WD J1344−5738B	19.8849 ± 0.0045	...	...	...	...	18.8040 ± 0.0095	17.4591 ± 0.0056	16.8306 ± 0.0078	5	
WD J1418+0929B	...	...	...	...	>24.4540	>22.0270	20.9369 ± 0.0370	19.5623 ± 0.0250	18.6138 ± 0.0178	2
WD J1642+5151B	...	...	...	...	>21.7110	>20.2500	20.8786 ± 0.0226	19.4321 ± 0.0127	18.4942 ± 0.0232	2
WD J1715−1910B	19.8196 ± 0.0048	21.7778 ± 0.2158	18.1524 ± 0.0310	>20.8400	>19.1840	19.3805 ± 0.0242	17.8437 ± 0.0077	17.0125 ± 0.0093	2	
WD J2005+6932B	19.7230 ± 0.0046	21.0920 ± 0.3113	18.1748 ± 0.0298	...	...	19.1485 ± 0.0123	17.7141 ± 0.0099	16.9559 ± 0.0089	2	
WD J2025+3515B	20.0151 ± 0.0050	21.5649 ± 0.1600	18.4568 ± 0.0198	>20.5270	>18.9160	19.4778 ± 0.0239	18.0853 ± 0.0082	17.3116 ± 0.0101	2	
WD J2119+4206B	20.3323 ± 0.0064	21.6090 ± 0.3051	18.7856 ± 0.0219	...	21.0458 ± 0.0794	19.8073 ± 0.0140	18.3919 ± 0.0089	17.5155 ± 0.0105	2	
WD J2353−4325B	...	...	...	27.5550 ± 4.6653	24.3429 ± 0.3295	24.0255 ± 0.4225	21.5718 ± 0.0873	20.9234 ± 0.1308	1	
WD J2355+5131B	20.4489 ± 0.0059	21.2955 ± 0.1300	18.8772 ± 0.0255	...	...	19.9599 ± 0.0332	18.5047 ± 0.0144	17.7087 ± 0.0171	2	

References—(1) The Dark Energy Survey (DES; The Dark Energy Survey Collaboration 2005); (2) PS1 (Chambers et al. 2016); (3) DESI Legacy Imaging Surveys (Dey et al. 2019); (4) SkyMapper (Wolf et al. 2018); (5) NSC DR2 (Nidever et al. 2021)

### 3. OBSERVATIONS

#### 3.1. IRTF/SpeX

Four of our resolved candidate companions were observed with the SpeX spectrograph (Rayner et al. 2003) at NASA’s Infrared Telescope Facility (IRTF). Observations for WD J0806+2215B were taken on 11 November 2018 and for WD J2025+3515B, WD J2119+4206B, and WD J2355+5131B on 13 August 2024. All observations were done in prism mode with the  $0''.8$  slit, which results in a resolving power of  $\approx 200$  across  $0.8\text{--}2.5 \mu\text{m}$ . The spectra were reduced using the Spextool reduction package (Cushing et al. 2004; Vacca et al. 2003). The final reduced spectra is shown in Figure 4. Comparing to near-infrared L and T dwarf spectral standards from Burgasser et al. (2006) and Kirkpatrick et al. (2010), we find that the best match at the *J*-band for WD J0806+2215B is the L3 standard (2MASSW J1506544+132106; Burgasser 2007). For WD J2025+3515B, WD J2119+4206B, and WD J2355+5131B, we find the best matching standard at *J*-band to be the M8 standard (VB 10; Burgasser et al. 2004).

#### 3.2. Gemini/GMOS

One white dwarf primary (WD J0400–2611) was observed with the Gemini-North Multi-Object Spectrograph (GMOS; Hook et al. 2004) as part of program GN-2021A-Q-316 (PI: Debes). WD J0400–2611 was observed with the R400 grating using the  $1''$  slit with  $2\times 2$  binning centered on  $0.764 \mu\text{m}$ . The purpose of this observation was to examine the spectrum for the presence of hydrogen or helium to determine whether this object had a DA or non-DA composition. We obtained 4,300 s exposures that were then stacked during the reduction. The spectra were reduced using the DRAGONS reduction software (Labrie et al. 2019, 2023), which performs the bias, flat-field, bad pixel and wavelength corrections as well as the response function determined from a standard star. The  $\text{H}\alpha$  absorption line, which indicates that this object is a DA white dwarf, is shown in Figure 5.

### 4. SYSTEM PROPERTIES

#### 4.1. $T_{\text{eff}}$ and $\log(g)$

We gathered the basic fundamental properties of all candidate systems by searching the literature for  $T_{\text{eff}}$  and  $\log(g)$  values of the primary white dwarf and taking

the most precise values available if more than one estimate existed. Most of these measurements come from newly available low-resolution Gaia XP spectra (e.g., Jiménez-Esteban et al. 2023; Vincent et al. 2024). These values are provided in Table 8.

#### 4.2. Spectral Types

We searched the literature for spectral types for the candidate unresolved systems and the white dwarf primaries of resolved co-moving systems. Spectral types, including our type found for WD J0400–2611 from Section 3, are given in Table 8.

#### 4.3. Ages

We determined age estimates for all of our candidate systems using `wdwarfdate` (Kiman et al. 2022). `wdwarfdate` estimates the total ages of white dwarfs by combining their cooling ages with the main-sequence lifetimes of their progenitor stars. It uses the Initial-to-Final Mass Relation (IFMR), and in this study, we used the highest-accuracy Cummings et al. (2018) (both MIST and PARSEC-based), which links the white dwarf’s mass to the mass of its progenitor. The package incorporates cooling models from Bédard et al. (2020) which detail the cooling process of white dwarfs based on their mass, temperature, and atmospheric composition. The package also incorporates stellar evolution models from Dotter (2016) and Choi et al. (2016) to estimate the main-sequence lifetime of the progenitor star. `wdwarfdate` also handles DA and non-DA white dwarfs differently. For DA white dwarfs, the models from Bédard et al. (2020) address their slower cooling rates, considering that the hydrogen layer is more insulating than a non-DA helium counterpart (Fontaine et al. 2001). These non-DA counterparts also have their own distinct cooling model, so as to best estimate an age with models most representative of the actual composition of the object. If no spectral type was found for an object in our sample, we evaluate both DA and non-DA ages for that system. Some objects had conflicting spectral types in the literature (e.g., WD J001419.17–475719.58 is typed as non-DA in Jiménez-Esteban et al. 2023 and DA in Vincent et al. 2024). In these cases, we evaluate both DA and non-DA scenarios and provide both age estimates.

Ages or age limits were determined for all but four of the unresolved candidates (Table 8). WD J1628–0418, WD J1657–1256, and WD J2053+2603 had no available  $T_{\text{eff}}$  or  $\log(g)$  values available in the literature, and WD J2339+2552 has an unusually low  $\log(g)$  value ( $6.88\pm 0.02$ ; Vincent et al. 2024) that is beyond the allowed values of the models considered by `wdwarfdate`.

**Table 6.** Infrared Photometry for Resolved Companions

WD Name	<i>J</i>	<i>H</i>	<i>K</i>	NIR Source	<i>W1</i>	<i>W2</i>
	(mag)	(mag)	(mag)		(mag)	(mag)
WD J0012–4924B	17.419±0.025	16.987±0.044	16.592±0.053	1	16.437±0.032	16.269±0.074
WD J0014–4757B	15.790±0.006	15.210±0.006	14.709±0.008	1	14.320±0.014	14.204±0.015
WD J0149–6129B	15.938±0.007	...	15.126±0.013	1	14.746±0.014	14.391±0.015
WD J0230–3447B	14.951±0.040	14.355±0.044	13.913±0.051	2	13.740±0.015	13.513±0.012
WD J0237–1932B	14.748±0.004	...	13.877±0.006	1	13.685±0.015	13.476±0.012
WD J0324+6020B	16.626±0.126	15.841±0.155	15.091±0.117	2	17.528±0.086	17.784±0.297
WD J0356+3212B	18.367±0.074	...	17.398±0.064	3	...	...
WD J0400–2611B	16.543±0.008	...	15.517±0.018	1	15.136±0.018	14.977±0.026
WD J0426+4044B	...	...	15.285±0.009	3	14.898±0.017	14.821±0.027
WD J0447–5823B	15.258±0.004	...	14.384±0.007	1	14.177±0.012	13.960±0.011
WD J0525–1323B	15.167±0.004	...	14.350±0.008	1	14.066±0.015	13.876±0.015
WD J0652+5628B	16.834±0.021	...	15.614±0.028	4	15.211±0.022	15.046±0.028
WD J0716+0038B	16.540±0.016	...	15.440±0.022	4	15.125±0.018	15.128±0.033
WD J0735–7944B	18.568±0.092	...	17.452±0.159	1	17.083±0.052	16.985±0.123
WD J0806+2215B	16.988±0.153	15.847±0.131	14.901±0.111	2	14.406±0.017	14.227±0.019
WD J0807–5350B	15.902±0.010	...	15.024±0.017	1	14.630±0.014	14.371±0.015
WD J0813–1358B	16.615±0.010	...	15.486±0.079	1	15.056±0.018	14.924±0.027
WD J0824–2546B	15.959±0.008	...	15.080±0.016	1	14.723±0.021	14.535±0.023
WD J0950+1309B	17.871±0.033	17.265±0.043	16.989±0.064	3	...	...
WD J1046+6054B	14.534±0.030	13.876±0.041	13.358±0.033	2	13.041±0.011	12.825±0.009
WD J1234+4427B	17.788±0.044	...	17.020±0.067	4	16.721±0.035	16.423±0.077
WD J1250+4152B	17.592±0.037	...	16.623±0.062	4	16.056±0.025	15.825±0.043
WD J1344–5738B	15.611±0.083	14.993±0.095	14.924±0.141	2	14.272±0.013	14.260±0.015
WD J1418+0929B	16.613±0.010	15.905±0.011	15.313±0.012	3	15.092±0.026	14.935±0.034
WD J1642+5151B	16.753±0.127	16.178±0.201	...	2	15.218±0.015	14.944±0.019
WD J1715–1910B	15.262±0.005	...	14.286±0.008	1	13.872±0.018	13.655±0.016
WD J2005+6932B	...	...	...	...	14.102±0.013	13.828±0.011
WD J2025+3515B	15.600±0.005	...	...	3	14.041±0.043	13.826±0.043
WD J2119+4206B	15.826±0.005	...	14.668±0.007	3	14.555±0.018	14.413±0.022
WD J2353–4325B	18.901±0.050	...	18.738±0.247	1	17.206±0.056	16.177±0.063
WD J2355+5131B	16.021±0.010	...	14.967±0.013	4	14.751±0.017	14.546±0.019

**References**—(1) VHS (McMahon et al. 2013); (2) 2MASS (Skrutskie et al. 2006); (3) UKIDSS (Lawrence et al. 2007); (4) UHS (Dye et al. 2018)

(Kiman et al. 2022). Ages or age limits are estimated for all thirty-one resolved candidate systems (Table 8).

## 5. ANALYSIS

### 5.1. Spectral Binaries

Several objects (WD J1125–1631AB, WD J1657–1256AB, and WD J2339+2552AB) have available optical spectra from Gaia DR3 (Gaia Collaboration et al. 2021a; De Angeli et al. 2023). We extracted each available spectrum using the GaiaXPy Python library (Ruz-Mieres & Zuzannakr 2024). We inspected each spectrum for potential spectral signatures of low-mass companions. Three objects (WD J1125–1631, WD J1657–1256, and WD J2339+2552) showed clear signs of unresolved binarity with a low-mass companion. We made templates using spectroscopically classified white dwarfs from McCook & Sion (1999) and M and L dwarf standards (Kirkpatrick et al. 1991, 1999). All of the

spectra were absolutely flux-calibrated using Gaia DR3 parallaxes, however we allow for additional multiplicative coefficients to the white dwarf, M dwarf, and L dwarf templates to allow for unaccounted flux discrepancies such as variability or additional unresolved binarity of either the standard or the candidates. The best fitting templates were found via  $\chi^2$ -fitting to the white dwarf + cool dwarf templates. The white dwarfs used in the final fits are GD 140 (DA3; McCook & Sion 1999), EGGR 155 (DA5; McCook & Sion 1999), and EGGR 7 (DA6; McCook & Sion 1999), while the M dwarfs are Gl 402 (M4; Kirkpatrick et al. 1991) and VB 8 (M7; Henry et al. 2004). The best fitting templates to the Gaia spectra of WD J1125–1631, WD J1657–1256, and WD J2339+2552 are shown in Figure 6.

### 5.2. Old Systems

**Table 7.** Candidate Companion Spectral Types

WD Name	$M_G$	$M_J$	$M_K$	Spectral <sup>a</sup>
	(mag)	(mag)	(mag)	Type
WD J0012–4924B	16.191±0.090	12.505±0.093	11.678±0.104	[L3]
WD J0014–4757B	15.676±0.131	11.141±0.131	10.060±0.131	[M8]
WD J0149–6129B	16.176±0.104	11.540±0.104	10.728±0.105	[L0]
WD J0230–3447B	14.659±0.034	10.651±0.052	9.613±0.061	[M7]
WD J0237–1932B	14.371±0.029	10.391±0.029	9.520±0.030	[M7]
WD J0324+6020B	...	12.493±0.126	10.958±0.117	[L2]
WD J0356+3212B	...	13.551±0.082	12.582±0.074	[L6]
WD J0400–2611B	...	11.572±0.048	10.546±0.051	[L0]
WD J0426+4044B	...	...	10.534±0.036	[L0]
WD J0447–5823B	14.656±0.046	10.633±0.046	9.759±0.046	[M7]
WD J0525–1323B	14.805±0.059	10.712±0.059	9.895±0.060	[M7]
WD J0652+5628B	...	11.858±0.078	10.638±0.081	[L1]
WD J0716+0038B	...	11.550±0.128	10.450±0.128	[L0]
WD J0735–7944B	...	13.648±0.092	12.532±0.159	[L6]
WD J0807–5350B	16.321±0.172	11.601±0.171	10.723±0.172	[L0]
WD J0813–1358B	...	12.195±0.027	11.066±0.083	[L1]
WD J0824–2546B	15.109±0.139	10.946±0.139	10.067±0.140	[M8]
WD J0950+1309B	...	14.118±0.038	13.236±0.067	[L8]
WD J1234+4427B	...	12.817±0.084	12.049±0.098	[L3]
WD J1250+4152B	...	12.601±0.178	11.632±0.185	[L3]
WD J1344–5738B	15.231±0.082	10.957±0.117	10.270±0.163	[M8]
WD J1418+0929B	...	11.924±0.013	10.624±0.015	[L1]
WD J1642+5151B	...	11.790±0.150	...	[L0]
WD J1715–1910B	15.811±0.063	11.254±0.063	10.278±0.063	[M9]
WD J2005+6932B	15.555±0.043	...	...	[M9]
WD J2353–4325B	...	14.648±0.094	...	[T5]
WD J0806+2215B	...	13.518±0.154	11.431±0.112	L3
WD J1046+6054B	15.586±0.021	11.204±0.037	10.028±0.039	M9 <sup>b</sup>
WD J2025+3515B	15.192±0.085	10.777±0.085	...	M8
WD J2119+4206B	15.662±0.104	11.155±0.104	9.997±0.104	M8
WD J2355+5131B	15.615±0.144	11.187±0.144	10.133±0.145	M8
WD J1125–1631B	...	...	...	M7 <sup>c</sup>
WD J1657–1256B	...	...	...	M4 <sup>c</sup>
WD J2339+2552B	...	...	...	M7 <sup>c</sup>

<sup>a</sup>Spectral types in square brackets are estimates based on the absolute magnitudes listed and spectral type versus absolute magnitude relations from Pecaut & Mamajek (2013), Kiman et al. (2019), and Schneider et al. (2023), while those spectral types without square brackets are those that have been confirmed spectroscopically.

<sup>b</sup> WD J1046+6054B has an optical spectral type of M9 from Kiman et al. (2019).

<sup>c</sup> These spectral types were determined via spectral decomposition in Section 5.1.

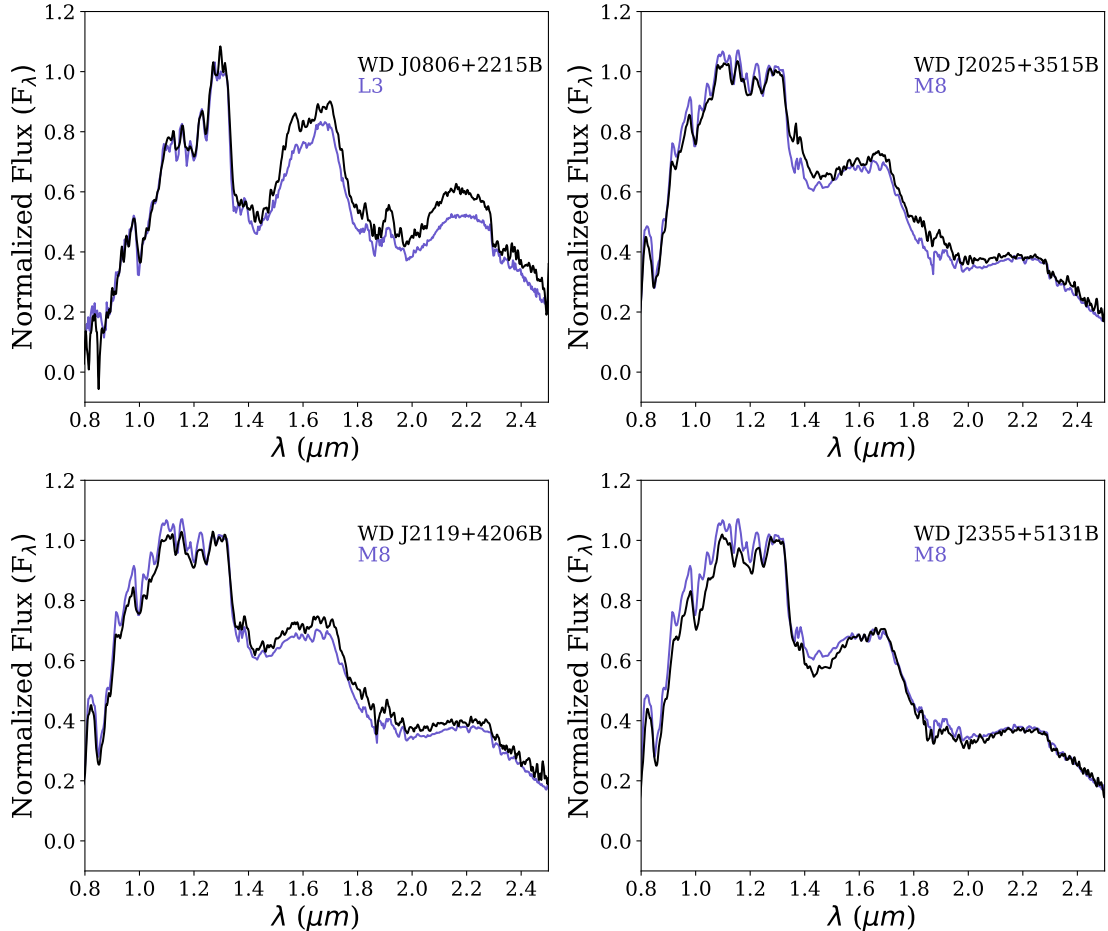


**Figure 4.** IRTF/SpeX spectra of four newly discovered companions. All spectra are normalized between 1.27 and 1.29  $\mu\text{m}$ . WD J0806+2215B is best matched to the L3 spectral standard (2MASSW J1506544+132106; [Burgasser 2007](#)), while WD J2025+3515B, WD J2119+4206B, and WD J2355+5131B are best matched to the M8 spectral standard (VB 10; [Burgasser et al. 2004](#)).

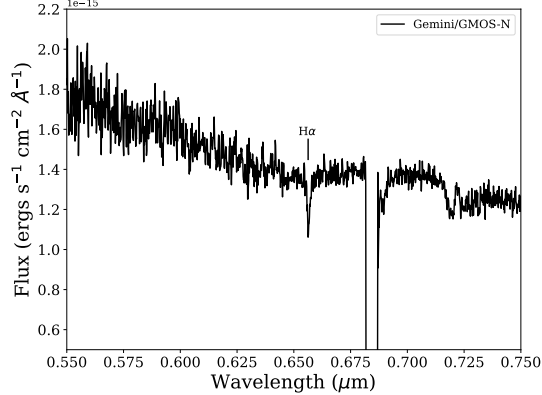


**Figure 5.** Gemini/GMOS-N spectrum of WD J0400–2611 showing clear H $\alpha$  absorption and a lack of He lines.

WD J0012–4924AB, WD J0824–2546AB, WD J1046+6054AB, WD J1715–1910AB, WD J2005+6932AB, and WD J2353–4325AB all have age estimates  $>10$  Gyr, making them potential benchmark systems with advanced ages.

WD J1046+6054B has a confirmed optical spectral type of M9 from [Kiman et al. \(2019\)](#). While no suggestion of low-metallicity was made for this source in that work, the calculated tangential velocity ( $V_{\tan}$ ) of  $\sim 250$  km s $^{-1}$  supports the old age estimate for this system. WD J0824–2546B, WD J1715–1910B, WD J2005+6932B all have estimated spectral types of late-M similar to WD J1046+6054B. The WD J1715–1910AB system may be particularly valuable with the oldest age estimate in the entire sample presented in this work ( $11.83^{+2.10}_{-2.08}$  Gyr).

WD J0012–4924AB is a system that needs future astrometric confirmation of the physical association of the potential companion and the white dwarf. If confirmed, the candidate companion has an estimated spectral type of  $\sim$ L3. Follow-up spectroscopy could reveal this as a potential benchmark system containing an L subdwarf with a well-constrained age, joining a relatively rare group that includes VVV 1256–62AB ([Zhang et al. 2024b](#)).

WD J2353–4325A does not have a confirmed white dwarf spectral type, but has an age of  $11.12^{+2.03}_{-1.92}$  Gyr based on the DA cooling model and  $9.92^{+2.90}_{-1.27}$  Gyr based on the non-DA model. The companion in this system, WD J2353–4325B, has a spectral type estimate of  $\sim$ T5. Therefore this system could be especially valuable as it contains a mid-T dwarf with an exceptionally old age. The cloudless Sonora models ([Marley et al. 2021](#)) give a mass estimate of  $70.4 \pm 3.3 M_{\text{Jup}}$  and  $69.9 \pm 2.8 M_{\text{Jup}}$  for a T5 dwarf at the DA and non-DA age of the primary, respectively.

### 5.3. Notes on Individual Systems

#### 5.3.1. WD J0004+7401

Confirmation of infrared excess with higher resolution follow-up infrared imaging (e.g., [Lai et al. 2021](#)) or additional photometric detections at longer wavelengths for this unresolved source can help to distinguish between true infrared excess due to a dusty debris disk or some contaminating flux from another source. None of our seventeen excess systems have additional infrared imaging from the Spitzer Space Telescope in the Spitzer Heritage Archive ([Wu et al. 2010](#)). We further looked for longer wavelength detections at  $12\text{ }\mu\text{m}$  and  $22\text{ }\mu\text{m}$  in the AllWISE catalog ([Kirkpatrick et al. 2014](#)), as the CatWISE2020 catalog only includes W1 and W2 photometry ([Marocco et al. 2021](#)). Only three objects have  $12\text{ }\mu\text{m}$  (W3) detections (WD J0004+7401, WD J1125–1631, and WD J1657–1256), and there are no detections at  $22\text{ }\mu\text{m}$  (W4). The W3 detections of WD J1125–1631 and WD J1657–1256 are most likely due to unresolved stellar companions, as discussed in the next paragraph. The W3 detection of WD J0004+7401 may be evidence of circumstellar material for this source. Its extra-red nature is visible in Figure 2, with a reddish hue in the WISE composite image that is not seen for the other sources in that figure due to the brighter than typical W3 flux for this source. Confirmation is possible with future high-resolution infrared images or mid- to far-infrared spectroscopy. The total age for this white dwarf is  $>5.64^{+4.57}_{-2.38}$  Gyr if a hydrogen dominated atmosphere and  $>6.08^{+2.05}_{-2.69}$  Gyr in the non-DA case. With a  $T_{\text{eff}} \sim 4300$ –4400 K, this would be one of the coldest and oldest white dwarfs to show infrared excess due to a dusty disk (e.g., [Debes et al. 2019](#)).

#### 5.3.2. WD J0024–1631

This unresolved source is almost certainly a white dwarf + low-mass companion system, as a very red point source can be seen blended with the white dwarf primary in the PS1 images in Figure 2. However, this source was not resolved into two detections in the PS1 DR2 catalog at this position. Because this pair was not resolved in any existing catalog, it is included in our list of unresolved candidates. High-resolution imaging of this system and any resulting unblended photometry would allow for an accurate spectral type estimate for this companion.

#### 5.3.3. WD J0735–7944AB

This white dwarf in this resolved system has the highest  $T_{\text{eff}}$  in our sample ( $28063 \pm 836$  K; [Jiménez-Esteban et al. 2023](#)) and consequently has the youngest age estimate ( $0.21 \pm 0.02$  Gyr). The high  $T_{\text{eff}}$  of this source

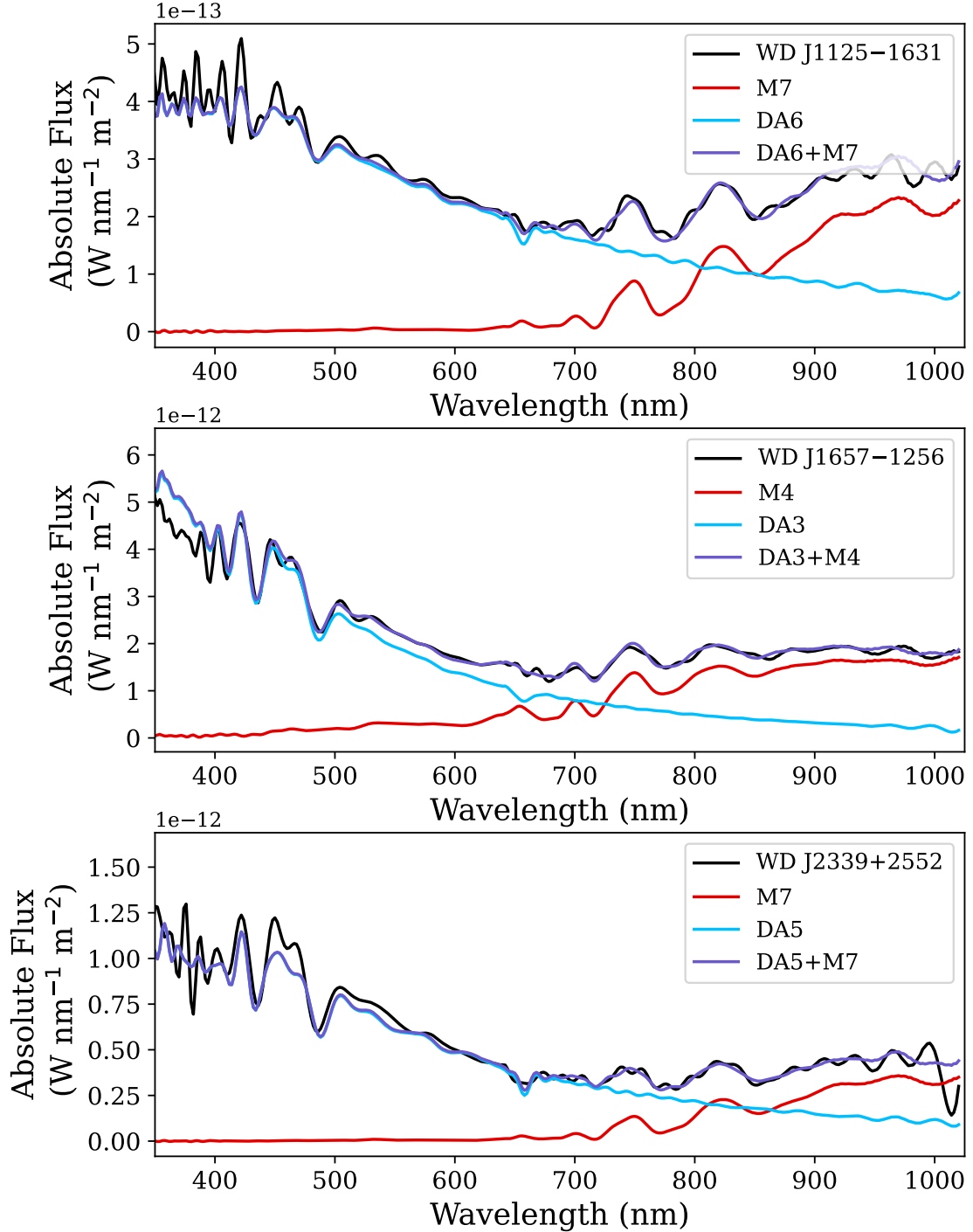


**Figure 6.** Spectral binary fits to the Gaia spectra of WD J1125–1631, WD J1657–1256, and WD J2339+2552. White dwarf spectra are shown in cyan, M dwarf spectra are shown in red, and the combined white dwarf + M dwarf templates are shown in purple. The observed Gaia spectra for these three unresolved candidates are shown in black.

is supported by the values reported in Gentile Fusillo et al. (2021) ( $28583 \pm 1173$  K) and Vincent et al. (2024) ( $35337 \pm 1290$  K). We note that this is one of our “unreliable” systems for which a detailed astrometric analysis of the potential companion is needed. However, if confirmed, we estimate a spectral type of  $\sim$ L6 for the putative companion. At the age of WD J0735–7944A, an L6 companion would have a mass of  $34 \pm 5 M_{\text{Jup}}$  according to the solar metallicity hybrid-grav Sonora Diamond-back models from Morley et al. (2024).

### 5.3.4. WD J0806+2215AB

The companion in this resolved system was observed with IRTF/SpeX (Figure 4) and was found to have a spectral type of L3. The spectrum is slightly redder than the L3 standard, which is unlikely to be related to a young age (i.e., low surface gravity), as the age of the system is found to be  $5.56^{+3.08}_{-0.98}$  Gyr. Other factors can cause redder colors, such as enhanced metallicity (e.g., Looper et al. 2008; Zhang et al. 2024a) or inclination angle (e.g., Vos et al. 2017; Suárez et al. 2023). We find a  $T_{\text{eff}}$  of  $1841 \pm 147$  K using the spectral type vs.  $T_{\text{eff}}$  relations from Kirkpatrick et al. (2021), leading to a mass

estimate of  $77.4 \pm 2.6 M_{\text{Jup}}$  using the age of the system and the solar-metallicity hybrid-grav models of Morley et al. (2024). This is just above the hydrogen burning limit for the hybrid models ( $70.2 M_{\text{Jup}}$ ; Morley et al. 2024) making this a likely low-mass, stellar companion.

### 5.3.5. WD J0950+1309AB

Of the remaining resolved candidates with reliable astrometry that give a high probability of physical association with a white dwarf primary not already discussed previously, WD J0950+1309B is the lone object with a spectral type estimate clearly in the substellar regime ( $\sim$ L8). Spectroscopic confirmation for the primary and secondary are needed for this system, which could become a benchmark object with a well-determined age at the L/T transition.

### 5.3.6. WD J2119+4206

The possible companion in this resolved system is all but ruled-out as physically associated by the CoMover results in Table 4. The companion candidate was followed-up spectroscopically (Section 3) before being evaluated with CoMover, and found to have a spectral type of M8. This system is likely a chance alignment.

**Table 8.** Age Estimates for All Candidates

	Spectral	Ref.	$T_{\text{eff}}$	$\log(g)$	Ref.	Age
	Type		(K)	(cgs)		(Gyr)
WD J0004+7401	[DA]	...	$4289 \pm 426$	$7.82 \pm 0.39$	8	$>5.64^{+4.57}_{-2.38}$
	[non-DA]	...	$4392 \pm 307$	$7.85 \pm 0.36$	8	$>6.08^{+2.05}_{-2.69}$
WD J0012–4924	DA	1	$4720 \pm 111$	$8.05 \pm 0.07$	1	$10.82^{+2.42}_{-1.26}$
WD J0014–4757	DA	1	$6420 \pm 93$	$8.24 \pm 0.03$	1	$3.93^{+0.29}_{-0.27}$
	non-DA	2	$6035 \pm 125$	$8.15 \pm 0.05$	2	$5.26^{+2.25}_{-0.71}$
WD J0024–1631	DA	1	$4608 \pm 150$	$7.77 \pm 0.09$	1	$>4.18^{+1.03}_{-0.72}$
WD J0045+1454	DA	3	$6963 \pm 77$	$8.38 \pm 0.02$	1	$3.80^{+0.15}_{-0.16}$
WD J0127–5759	DA	2	$15888 \pm 426$	$8.95 \pm 0.02$	1	$1.07^{+0.09}_{-0.08}$
WD J0149–6129	DQ	1	$8581 \pm 72$	$7.89 \pm 0.02$	1	$>0.84^{+0.02}_{-0.03}$
WD J0230–3447	DA	1	$4760 \pm 92$	$7.84 \pm 0.06$	1	$>4.26^{+0.88}_{-0.58}$
WD J0237–1932	DA	1	$5079 \pm 127$	$8.01 \pm 0.07$	1	$9.84^{+3.08}_{-2.00}$
WD J0324+6020	DA	1	$10960 \pm 76$	$8.03 \pm 0.01$	1	$3.67^{+3.94}_{-1.55}$
WD J0356+3212	DA	1	$8040 \pm 223$	$8.56 \pm 0.04$	1	$3.32^{+0.27}_{-0.26}$
WD J0400–2611	DA	11	$5688 \pm 89$	$8.00 \pm 0.04$	1	$7.58^{+4.06}_{-2.41}$
WD J0426+4044	DA	2	$6395 \pm 94$	$7.98 \pm 0.03$	1	$7.69^{+3.78}_{-2.91}$
WD J0447–5823	DA	2	$7630 \pm 110$	$7.99 \pm 0.03$	1	$6.95^{+4.64}_{-3.04}$
WD J0525–1323	DA	1	$5211 \pm 71$	$7.32 \pm 0.05$	1	$>1.77^{+0.12}_{-0.26}$
WD J0609–3035	DA	1	$4848 \pm 103$	$7.86 \pm 0.06$	1	$>4.21^{+0.85}_{-0.61}$

**Table 8** *continued*

**Table 8** (*continued*)

	Spectral Type	Ref.	$T_{\text{eff}}$ (K)	$\log(g)$ (cgs)	Ref.	Age (Gyr)
WD J0642–4721	DA	1	4450±163	7.63±0.11	1	$>3.66^{+0.92}_{-0.62}$
WD J0652+5628	DA	1	6048±196	8.16±0.07	1	$4.69^{+1.46}_{-0.66}$
WD J0716+0038	[DA]	...	4946±450	7.80±0.43	8	$>3.79^{+4.55}_{-1.70}$
	[non-DA]	...	4925±380	7.82±0.38	8	$>4.21^{+2.90}_{-1.86}$
WD J0735–7944	DA	2	28063±836	8.86±0.03	2	$0.21^{+0.02}_{-0.02}$
WD J0806+2215	DA	4	5760±35	8.07±0.02	9	$5.56^{+3.08}_{-0.98}$
WD J0807–5350	DA	1	4433±125	7.53±0.09	1	$>3.25^{+0.57}_{-0.40}$
WD J0813–1358	non-DA	2	6451±131	7.97±0.04	1	$8.71^{+3.36}_{-3.15}$
WD J0824–2546	DA	1	5081±136	7.92±0.08	1	$10.60^{+2.85}_{-2.50}$
WD J0950+1309	DA	1	5968±85	8.20±0.03	1	$4.64^{+0.40}_{-0.33}$
	non-DA	2	5770±128	8.16±0.06	2	$6.10^{+2.32}_{-0.77}$
WD J1042+3422	DA:	1	5510±155	8.58±0.07	1	$7.82^{+0.69}_{-0.68}$
WD J1046+6054	DC:	1	5162±39	8.00±0.02	1	$10.81^{+2.34}_{-2.33}$
WD J1125–1631	DA	1	6514±25	7.06±0.01	1	$>0.63^{+0.02}_{-0.01}$
WD J1157+0631	DA	5	7871±26	7.49±0.08	7	$>0.69^{+0.05}_{-0.06}$
WD J1234+4427	DA	1	5384±126	8.11±0.07	1	$7.17^{+2.81}_{-1.18}$
WD J1250+4152	[DA]	...	4060±680	7.84±0.66	10	$>7.53^{+3.69}_{-4.17}$
	[non-DA]	...	4098±375	7.78±0.56	8	$>6.59^{+2.01}_{-3.05}$
WD J1344–5738	DA	1	5733±88	7.79±0.04	1	$>2.22^{+0.27}_{-0.28}$
WD J1418+0929	DA	6	15572±149	7.93±0.01	1	$7.08^{+4.18}_{-3.37}$
WD J1421+1436	DA	7	5407±99	7.27±0.25	7	$>1.58^{+0.44}_{-0.30}$
WD J1505+3304	DA:	1	4299±178	7.62±0.12	1	$>4.01^{+0.96}_{-0.72}$
WD J1628–0418	...	...	...	...	...	...
WD J1642+5151	[DA]	...	5125±419	8.21±0.33	8	$9.08^{+2.85}_{-2.27}$
	[non-DA]	...	5020±377	8.14±0.32	8	$8.79^{+3.44}_{-1.56}$
WD J1657–1256	DA	1	...	...	...	...
WD J1715–1910	DA:	1	4755±110	7.93±0.06	1	$11.83^{+2.10}_{-2.08}$
WD J2005+6932	DA:	1	4937±99	8.02±0.05	1	$10.54^{+2.72}_{-1.86}$
WD J2025+3515	DA	2	8293±105	8.02±0.02	1	$5.35^{+4.70}_{-2.32}$
WD J2051–3558	DA	2	9053±114	8.23±0.02	1	$1.68^{+0.22}_{-0.11}$
WD J2053+2603	...	...	...	...	...	...
WD J2119+4206	DA	2	11691±111	7.81±0.01	2	$>0.32^{+0.01}_{-0.01}$
WD J2339+2552	DA	1	7489±47	6.88±0.02	1	...
WD J2353–4325	[DA]	...	4427±438	8.16±0.36	8	$11.13^{+2.03}_{-1.92}$
	[non-DA]	...	4422±343	8.10±0.35	8	$9.92^{+2.90}_{-1.27}$
WD J2355+5131	DA	1	5706±151	8.42±0.06	1	$6.53^{+0.71}_{-0.59}$
WD J2357+3043	DA:	1	5997±67	7.35±0.05	1	$>1.24^{+0.09}_{-0.11}$

NOTE—For objects with surface gravities outside of the lower limit of 7.9 set in [Kiman et al. \(2022\)](#), the cooling age is treated as a lower age limit.

**References**—(1) [Vincent et al. \(2024\)](#); (2) [Jiménez-Esteban et al. \(2023\)](#); (3) [Kleinman et al. \(2004\)](#); (4) [Limoges et al. \(2015\)](#); (5) [Girven et al. \(2011\)](#); (6) [Brown et al. \(2007\)](#); (7) [Kepler et al. \(2019\)](#); (8) [Gentile Fusillo et al. \(2021\)](#); (9) [Blouin et al. \(2019\)](#); (10) [Gentile Fusillo et al. \(2019\)](#); (11) This work.

## 6. CONCLUSIONS

In this study, we identified and compiled a new set of ultracool dwarf companions to white dwarfs within 100 pc using available astrometry and optical and infrared data. Through our search, we identified fifty-one previously unrecognized systems with candidate ultracool companions. Of these, thirty-one are resolved in at least one catalogue, with all but six reliably confirmed as co-moving based on consistent proper motion and parallax measurements (if available). The six unreliable cases will require additional astrometric data to verify their status as companions to the white dwarf primary.

Follow-up near-infrared spectroscopy of four of our resolved co-moving candidates confirmed their ultracool nature with three confirmed to be M8, and one a likely stellar source with an L3 spectral type. However, one of these systems (WD J2119+4206) was deemed unlikely to be physically associated in our astrometric analysis. Three of our unresolved sources were confirmed as having cool stellar companions via spectral decomposition of available optical spectra from Gaia. The remaining candidates will benefit from detailed follow-up spectroscopy to further constrain the natures of these systems.

## 7. ACKNOWLEDGEMENTS

The authors acknowledge support from the Science and Engineering Apprenticeship Program (SEAP) of the Office of Naval Research.

This publication makes use of data products from the *Wide-field Infrared Survey Explorer*, which is a joint project of the University of California, Los Angeles, and the Jet Propulsion Laboratory/California Institute of Technology, and NEOWISE which is a project of the Jet Propulsion Laboratory/California Institute of Technology. *WISE* and NEOWISE are funded by the National Aeronautics and Space Administration. Part of this research was carried out at the Jet Propulsion Laboratory, California Institute of Technology, under a contract with the National Aeronautics and Space Administration.

This publication makes use of data products from the UKIRT Hemisphere Survey, which is a joint project of the United States Naval Observatory, the University of Hawaii Institute for Astronomy, the Cambridge University Cambridge Astronomy Survey Unit, and the University of Edinburgh Wide-Field Astronomy Unit (WFAU). This project was primarily funded by the United States Navy. The WFAU gratefully acknowledges support for

this work from the Science and Technology Facilities Council through ST/T002956/1 and previous grants.

The Pan-STARRS1 Surveys (PS1) and the PS1 public science archive have been made possible through contributions by the Institute for Astronomy, the University of Hawaii, the Pan-STARRS Project Office, the Max-Planck Society and its participating institutes, the Max Planck Institute for Astronomy, Heidelberg and the Max Planck Institute for Extraterrestrial Physics, Garching, The Johns Hopkins University, Durham University, the University of Edinburgh, the Queen’s University Belfast, the Harvard-Smithsonian Center for Astrophysics, the Las Cumbres Observatory Global Telescope Network Incorporated, the National Central University of Taiwan, the Space Telescope Science Institute, the National Aeronautics and Space Administration under Grant No. NNX08AR22G issued through the Planetary Science Division of the NASA Science Mission Directorate, the National Science Foundation Grant No. AST-1238877, the University of Maryland, Eotvos Lorand University (ELTE), the Los Alamos National Laboratory, and the Gordon and Betty Moore Foundation.

This publication has made use of the Python package GaiaXPY, developed and maintained by members of the Gaia Data Processing and Analysis Consortium (DPAC), and in particular, Coordination Unit 5 (CU5), and the Data Processing Centre located at the Institute of Astronomy, Cambridge, UK (DPCI).

This research uses services or data provided by the Astro Data Lab, which is part of the Community Science and Data Center (CSDC) Program of NSF NOIRLab. NOIRLab is operated by the Association of Universities for Research in Astronomy (AURA), Inc. under a cooperative agreement with the U.S. National Science Foundation.

This work has benefitted from The UltracoolSheet at <http://bit.ly/UltracoolSheet>, maintained by Will Best, Trent Dupuy, Michael Liu, Aniket Sanghi, Rob Siverd, and Zhoujian Zhang, and developed from compilations by Dupuy & Liu (2012), Dupuy & Kraus (2013), Liu et al. (2016), Best et al. (2018), Best et al. (2021), Sanghi et al. (2023), and Schneider et al. (2023).

*Software:* CoMover (Gagné et al. 2021); GaiaXPY (Ruz-Mieres & Zuzannakr 2024); SpexTool (Cushing et al. 2004); WiseView (Caselden et al. 2018)

*Facilities:* Astro Data Lab, IRTF

## APPENDIX

### A. WHITE DWARF-WHITE DWARF SYSTEMS

Our search for cold companions using Gaia (Method III in Section 2) identified many likely white-dwarf-white dwarf systems. Listed in Table 9 are the 115 potential white dwarf-white dwarf systems found through our search where at least one component in the system has an absolute  $G$ -band magnitude  $>14.5$  mag.

**Table 9.** Candidate White Dwarf-White Dwarf Systems

WD Name	R.A. ( $^{\circ}$ )	Dec. ( $^{\circ}$ )	Sep. ( $''$ )	$\varpi$ (mas)	$\mu_{\alpha}$ (mas yr $^{-1}$ )	$\mu_{\delta}$ (mas yr $^{-1}$ )
WD J001440.69–075856.97	3.6703727	-7.9824549		10.7067 $\pm$ 0.2773	184.026 $\pm$ 0.304	8.642 $\pm$ 0.221
WD J001440.94–075857.72	3.6714185	-7.9826578	3.799	10.6252 $\pm$ 0.3461	184.174 $\pm$ 0.378	10.656 $\pm$ 0.282
WD J002229.32–723209.63	5.6244136	-72.5357083		11.2515 $\pm$ 0.0882	152.512 $\pm$ 0.121	67.550 $\pm$ 0.098
WD J002232.67–723233.64	5.6383606	-72.5423760	28.340	11.1783 $\pm$ 0.2545	152.169 $\pm$ 0.388	67.094 $\pm$ 0.298
WD J004920.31–833350.65	12.3369484	-83.5649155		17.9326 $\pm$ 0.1528	59.305 $\pm$ 0.190	-190.426 $\pm$ 0.181
WD J004922.35–833352.55	12.3454283	-83.5654492	3.924	18.1349 $\pm$ 0.1394	57.911 $\pm$ 0.168	-191.591 $\pm$ 0.169
WD J005133.15–671516.04	12.8890978	-67.2551668		11.1938 $\pm$ 0.2352	85.748 $\pm$ 0.288	-160.402 $\pm$ 0.283
WD J005134.57–671517.80	12.8950200	-67.2556566	8.429	11.3066 $\pm$ 0.3234	85.533 $\pm$ 0.376	-159.316 $\pm$ 0.388
WD J005550.32+854500.21	13.9825902	85.7509450		15.3529 $\pm$ 0.2100	381.124 $\pm$ 0.247	199.250 $\pm$ 0.244
WD J005551.69+854509.76	13.9883628	85.7535899	9.645	15.2162 $\pm$ 0.2253	382.152 $\pm$ 0.262	197.213 $\pm$ 0.272
WD J010456.47+211958.87	16.2342953	21.3311062		30.6583 $\pm$ 0.1101	-210.726 $\pm$ 0.141	-430.405 $\pm$ 0.095
WD J010457.96+212017.54	16.2404882	21.3362579	27.843	30.8044 $\pm$ 0.1138	-208.398 $\pm$ 0.147	-438.580 $\pm$ 0.101
WD J010903.42–104214.15	17.2650176	-10.7040573		16.4634 $\pm$ 0.0666	173.007 $\pm$ 0.095	-28.481 $\pm$ 0.107
WD J010904.22–104215.39	17.2683761	-10.7043972	11.943	16.7654 $\pm$ 0.2253	174.414 $\pm$ 0.366	-27.459 $\pm$ 0.355
WD J011728.64–043939.68	19.3681657	-4.6622002		24.2006 $\pm$ 0.1529	-264.474 $\pm$ 0.209	-264.895 $\pm$ 0.141
WD J011728.83–043938.41	19.3689792	-4.6618450	3.187	23.5673 $\pm$ 0.1535	-259.303 $\pm$ 0.201	-264.617 $\pm$ 0.142
WD J011911.55+312636.35	19.7971235	31.4429825		12.0849 $\pm$ 0.3719	-190.959 $\pm$ 0.368	-101.193 $\pm$ 0.282
WD J011911.80+312634.00	19.7981300	31.4423283	3.886	12.6415 $\pm$ 0.3856	-195.632 $\pm$ 0.381	-100.758 $\pm$ 0.295
WD J012327.62+390532.81	20.8652823	39.0920769		11.4706 $\pm$ 0.4602	36.599 $\pm$ 0.359	-85.683 $\pm$ 0.342
WD J012328.11+390530.76	20.8673707	39.0914859	6.211	11.2825 $\pm$ 0.5984	39.470 $\pm$ 0.491	-88.154 $\pm$ 0.450
WD J012621.66–611024.68	21.5916150	-61.1735373		12.4288 $\pm$ 0.1153	149.823 $\pm$ 0.111	-3.712 $\pm$ 0.109
WD J012622.26–611026.13	21.5941288	-61.1739247	4.581	12.3629 $\pm$ 0.3444	148.097 $\pm$ 0.320	0.649 $\pm$ 0.348
WD J013445.35+642959.71	23.6903081	64.5004880		13.0164 $\pm$ 0.2496	130.681 $\pm$ 0.192	128.128 $\pm$ 0.247
WD J013445.69+642953.22	23.6917507	64.4986718	6.910	12.4739 $\pm$ 0.2316	132.396 $\pm$ 0.182	124.772 $\pm$ 0.231
WD J015117.24+124106.19	27.8223269	12.6847248		10.7743 $\pm$ 0.4056	103.307 $\pm$ 0.483	-73.453 $\pm$ 0.444
WD J015117.40+124106.58	27.8229503	12.6848550	2.239	11.3616 $\pm$ 0.4448	98.577 $\pm$ 0.573	-71.234 $\pm$ 0.480
WD J021255.73–475803.38	33.2322541	-47.9675755		12.5863 $\pm$ 0.2404	8.070 $\pm$ 0.238	6.429 $\pm$ 0.249
WD J021255.95–475803.61	33.2331681	-47.9676311	2.212	13.2548 $\pm$ 0.2080	9.813 $\pm$ 0.208	8.480 $\pm$ 0.214
WD J022443.13–024255.30	36.1812965	-2.7149470		13.5405 $\pm$ 0.2844	359.925 $\pm$ 0.341	92.780 $\pm$ 0.249
WD J022443.44–024257.96	36.1825989	-2.7156982	5.408	13.4107 $\pm$ 0.2742	358.466 $\pm$ 0.316	89.655 $\pm$ 0.229
WD J022551.96+422803.52	36.4688877	42.4667255		19.7947 $\pm$ 0.0788	397.472 $\pm$ 0.091	-206.848 $\pm$ 0.086
WD J022552.59+422803.52	36.4715238	42.4667227	7.001	20.1056 $\pm$ 0.2148	399.941 $\pm$ 0.258	-207.737 $\pm$ 0.239
WD J023258.11–664822.91	38.2423462	-66.8066161		17.0207 $\pm$ 0.1038	21.131 $\pm$ 0.119	-56.449 $\pm$ 0.133
WD J023258.54–664817.55	38.2441728	-66.8051491	5.882	17.2730 $\pm$ 0.1444	23.430 $\pm$ 0.163	-61.066 $\pm$ 0.185
WD J024611.55–265128.81	41.5490878	-26.8573504		11.1575 $\pm$ 0.2104	191.524 $\pm$ 0.154	146.765 $\pm$ 0.196
WD J024612.62–265136.90	41.5535529	-26.8596060	16.480	12.0314 $\pm$ 0.5176	191.239 $\pm$ 0.384	146.596 $\pm$ 0.550
WD J025910.80–045531.15	44.7945286	-4.9258500		10.4737 $\pm$ 0.4913	-104.082 $\pm$ 0.504	-118.864 $\pm$ 0.530
WD J025910.81–045532.99	44.7945872	-4.9263602	1.848	12.5394 $\pm$ 0.4345	-99.357 $\pm$ 0.450	-119.470 $\pm$ 0.488

**Table 9** *continued*

**Table 9** (*continued*)

WD Name	R.A. ( $^{\circ}$ )	Dec. ( $^{\circ}$ )	Sep. ( $''$ )	$\varpi$ (mas)	$\mu_{\alpha}$	$\mu_{\delta}$
					(mas yr $^{-1}$ )	(mas yr $^{-1}$ )
WD J031945.74+640904.32	49.9426141	64.1510268		20.5635 $\pm$ 0.1207	199.488 $\pm$ 0.071	-38.548 $\pm$ 0.106
WD J031946.40+640854.18	49.9453785	64.1482168	11.007	20.5931 $\pm$ 0.1454	200.453 $\pm$ 0.088	-37.170 $\pm$ 0.132
WD J032414.19+611350.38	51.0586146	61.2304012		12.6170 $\pm$ 0.2636	-54.220 $\pm$ 0.285	-58.499 $\pm$ 0.315
WD J032414.66+611347.71	51.0606110	61.2296680	4.351	11.8883 $\pm$ 0.2757	-50.591 $\pm$ 0.295	-56.967 $\pm$ 0.331
WD J033304.60-563833.16	53.2694388	-56.6424918		10.6104 $\pm$ 0.0413	33.987 $\pm$ 0.048	12.067 $\pm$ 0.049
WD J033305.06-563833.52	53.2713546	-56.6425999	3.812	10.4286 $\pm$ 0.2843	32.774 $\pm$ 0.368	10.431 $\pm$ 0.342
WD J033649.70+641707.31	54.2080310	64.2846282		13.7655 $\pm$ 0.2684	92.680 $\pm$ 0.147	-164.991 $\pm$ 0.240
WD J033650.93+641709.86	54.2131407	64.2853412	8.384	13.8713 $\pm$ 0.1892	91.735 $\pm$ 0.102	-164.971 $\pm$ 0.174
WD J034501.53-034849.73	56.2563468	-3.8149903		32.2247 $\pm$ 0.1154	-8.806 $\pm$ 0.102	-264.757 $\pm$ 0.102
WD J034501.70-034844.85	56.2569717	-3.8136270	5.397	32.1842 $\pm$ 0.0820	-28.531 $\pm$ 0.074	-263.147 $\pm$ 0.072
WD J035012.13-383057.28	57.5505914	-38.5159057		11.3036 $\pm$ 0.1698	11.674 $\pm$ 0.160	1.050 $\pm$ 0.210
WD J035012.19-383051.98	57.5508536	-38.5144322	5.356	10.9623 $\pm$ 0.2555	10.929 $\pm$ 0.243	1.314 $\pm$ 0.329
WD J035656.96+521345.45	59.2376134	52.2285303		10.9369 $\pm$ 0.2482	39.435 $\pm$ 0.260	-171.191 $\pm$ 0.283
WD J035657.13+521345.97	59.2383243	52.2286519	1.628	11.6414 $\pm$ 0.2580	37.653 $\pm$ 0.277	-175.117 $\pm$ 0.283
WD J040229.20+481256.57	60.6225797	48.2147447		21.3730 $\pm$ 0.1226	138.754 $\pm$ 0.130	-218.119 $\pm$ 0.106
WD J040229.40+481256.62	60.6234670	48.2147260	2.129	21.6579 $\pm$ 0.1272	142.673 $\pm$ 0.142	-225.472 $\pm$ 0.110
WD J040952.26+195244.53	62.4677361	19.8786747		12.0577 $\pm$ 0.5616	-1.153 $\pm$ 0.513	-81.357 $\pm$ 0.464
WD J040952.71+195249.15	62.4696342	19.8799715	7.943	10.5242 $\pm$ 0.3761	-0.800 $\pm$ 0.388	-79.754 $\pm$ 0.347
WD J041612.00-822323.42	64.0519086	-82.3893146		17.3770 $\pm$ 0.1672	57.846 $\pm$ 0.234	118.378 $\pm$ 0.207
WD J041612.38-822326.26	64.0537485	-82.3900748	2.874	17.4722 $\pm$ 0.1765	64.543 $\pm$ 0.235	123.504 $\pm$ 0.218
WD J042029.21+261755.39	65.1213554	26.2985880		11.2535 $\pm$ 0.1570	-69.754 $\pm$ 0.201	-29.354 $\pm$ 0.151
WD J042031.95+261708.87	65.1327895	26.2856696	59.370	11.6084 $\pm$ 0.3722	-68.510 $\pm$ 0.477	-28.589 $\pm$ 0.355
WD J042535.48+021009.86	66.3983522	2.1695532		17.2978 $\pm$ 0.1930	114.372 $\pm$ 0.200	33.879 $\pm$ 0.158
WD J042535.86+021009.42	66.3999003	2.1694361	5.585	16.7394 $\pm$ 0.2105	112.336 $\pm$ 0.215	34.463 $\pm$ 0.170
WD J043726.68+291545.16	69.3615629	29.2621674		16.1993 $\pm$ 0.2221	79.593 $\pm$ 0.277	-85.011 $\pm$ 0.190
WD J043728.64+291522.49	69.3697597	29.2558761	34.289	16.5762 $\pm$ 0.2266	79.647 $\pm$ 0.285	-83.509 $\pm$ 0.196
WD J044457.95+093401.24	71.2417748	9.5669396		11.4687 $\pm$ 0.5674	69.953 $\pm$ 0.671	-15.633 $\pm$ 0.445
WD J044458.06+093403.60	71.2422082	9.5675986	2.828	11.3038 $\pm$ 0.5702	67.375 $\pm$ 0.661	-16.704 $\pm$ 0.416
WD J050517.30+192851.34	76.3230799	19.4805376		19.3568 $\pm$ 0.1995	215.007 $\pm$ 0.226	-87.868 $\pm$ 0.160
WD J050517.64+192844.93	76.3245093	19.4787709	7.999	19.6058 $\pm$ 0.1876	215.292 $\pm$ 0.214	-84.775 $\pm$ 0.152
WD J050640.18-551052.40	76.6682322	-55.1805613		10.2198 $\pm$ 0.0635	102.601 $\pm$ 0.076	148.630 $\pm$ 0.085
WD J050641.25-551129.39	76.6726869	-55.1908311	38.088	10.2629 $\pm$ 0.2738	102.844 $\pm$ 0.344	147.837 $\pm$ 0.408
WD J051250.01+473534.63	78.2080629	47.5909691		17.3859 $\pm$ 0.2164	-46.528 $\pm$ 0.267	-446.287 $\pm$ 0.232
WD J051251.03+473545.19	78.2123307	47.5939120	14.819	17.6029 $\pm$ 0.3755	-47.415 $\pm$ 0.458	-444.349 $\pm$ 0.402
WD J054705.48+753139.63	86.77755098	75.5275867		13.5239 $\pm$ 0.1874	150.647 $\pm$ 0.175	-20.102 $\pm$ 0.210
WD J054706.58+753103.10	86.7800858	75.5174347	36.778	13.2976 $\pm$ 0.1880	149.399 $\pm$ 0.165	-19.724 $\pm$ 0.205
WD J061209.21-734313.20	93.0389360	-73.7210593		11.3281 $\pm$ 0.2043	34.640 $\pm$ 0.231	-162.724 $\pm$ 0.233
WD J061209.44-734311.17	93.0398145	-73.7204831	2.256	11.4147 $\pm$ 0.2964	31.449 $\pm$ 0.347	-161.964 $\pm$ 0.333
WD J061806.18-110537.57	94.5249766	-11.0941059		16.8912 $\pm$ 0.2176	-169.017 $\pm$ 0.210	-75.674 $\pm$ 0.248
WD J061806.22-110541.87	94.5251738	-11.0952995	4.353	16.8600 $\pm$ 0.1811	-163.065 $\pm$ 0.171	-75.551 $\pm$ 0.209
WD J063347.72+341532.56	98.44486852	34.2592127		10.7504 $\pm$ 0.5436	-30.148 $\pm$ 0.545	37.643 $\pm$ 0.458
WD J063348.21+341536.93	98.4507325	34.2604230	7.489	11.1398 $\pm$ 0.3988	-29.361 $\pm$ 0.392	36.116 $\pm$ 0.330
WD J070326.09+622251.24	105.8576427	62.3799757		12.2384 $\pm$ 0.0342	-110.722 $\pm$ 0.033	-208.158 $\pm$ 0.030
WD J070326.56+622253.41	105.8596145	62.3805775	3.940	11.2593 $\pm$ 0.5696	-109.421 $\pm$ 0.546	-208.207 $\pm$ 0.494
WD J071038.98-644643.37	107.6621750	-64.7775440		11.9505 $\pm$ 0.1501	-23.050 $\pm$ 0.224	263.060 $\pm$ 0.164

**Table 9** *continued*

**Table 9** (*continued*)

WD Name	R.A.	Dec.	Sep.	$\varpi$	$\mu_\alpha$	$\mu_\delta$
					(°)	(°)
				(")	(mas)	(mas yr $^{-1}$ )
WD J071039.37–644646.89	107.6637879	-64.7785290	4.324	12.0441 $\pm$ 0.2487	-22.418 $\pm$ 0.370	261.238 $\pm$ 0.279
WD J074546.92–825400.39	116.4462945	-82.8996420		10.3798 $\pm$ 0.3848	20.152 $\pm$ 0.439	104.870 $\pm$ 0.379
WD J074548.49–825402.30	116.4528923	-82.9001779	3.513	10.1995 $\pm$ 0.3511	22.847 $\pm$ 0.406	104.988 $\pm$ 0.358
WD J075014.58+071148.92	117.5617156	7.1889986		54.9675 $\pm$ 0.0611	211.520 $\pm$ 0.071	-1782.618 $\pm$ 0.047
WD J075015.34+071137.10	117.5648647	7.1856806	16.407	55.1048 $\pm$ 0.0557	209.910 $\pm$ 0.068	-1790.496 $\pm$ 0.044
WD J075442.93–032224.13	118.6781482	-3.3731744		15.7229 $\pm$ 0.3192	-160.882 $\pm$ 0.309	44.037 $\pm$ 0.223
WD J075443.04–032228.99	118.6786196	-3.3745372	5.191	16.0783 $\pm$ 0.3182	-157.463 $\pm$ 0.297	40.750 $\pm$ 0.214
WD J080729.69–391206.96	121.8739434	-39.2018902		13.5017 $\pm$ 0.2196	37.888 $\pm$ 0.228	10.302 $\pm$ 0.278
WD J080730.53–391155.69	121.8774103	-39.1987706	14.821	13.3886 $\pm$ 0.2053	37.828 $\pm$ 0.207	7.570 $\pm$ 0.264
WD J082944.78–525705.69	127.4368508	-52.9519422		13.5560 $\pm$ 0.5197	38.460 $\pm$ 0.627	-81.206 $\pm$ 0.662
WD J082944.92–525707.51	127.4374067	-52.9524223	2.107	12.7794 $\pm$ 0.1816	32.774 $\pm$ 0.218	-76.525 $\pm$ 0.221
WD J083105.19–765253.79	127.7734957	-76.8820559		13.1626 $\pm$ 0.2610	96.458 $\pm$ 0.348	-101.377 $\pm$ 0.283
WD J083105.82–765251.63	127.7761478	-76.8814513	3.071	12.3257 $\pm$ 0.2441	95.969 $\pm$ 0.363	-99.739 $\pm$ 0.273
WD J092551.68+354000.58	141.4653750	35.6663662		14.4284 $\pm$ 0.1149	8.699 $\pm$ 0.140	-103.763 $\pm$ 0.153
WD J092551.76+353957.73	141.4657031	35.6655539	3.078	14.3515 $\pm$ 0.2314	10.340 $\pm$ 0.294	-108.278 $\pm$ 0.312
WD J094722.99+445948.59	146.8462272	44.9970255		18.5394 $\pm$ 0.2179	72.654 $\pm$ 0.203	43.308 $\pm$ 0.162
WD J094724.45+450001.85	146.8523191	45.0007018	20.388	18.1471 $\pm$ 0.1914	71.556 $\pm$ 0.176	42.095 $\pm$ 0.143
WD J100553.29–193056.55	151.4709362	-19.5152295		11.0226 $\pm$ 0.5048	-238.087 $\pm$ 0.490	107.920 $\pm$ 0.570
WD J100553.56–193055.83	151.4720682	-19.5150358	3.904	11.6713 $\pm$ 0.5403	-235.593 $\pm$ 0.541	105.383 $\pm$ 0.672
WD J100623.08+071212.70	151.5963157	7.2032200		18.3308 $\pm$ 0.0583	37.925 $\pm$ 0.061	-69.130 $\pm$ 0.059
WD J100623.17+071154.30	151.5967276	7.1981046	18.474	18.1518 $\pm$ 0.2255	37.308 $\pm$ 0.259	-70.214 $\pm$ 0.264
WD J101148.82+464929.83	152.9532581	46.8246483		10.8350 $\pm$ 0.3076	-25.295 $\pm$ 0.269	-68.902 $\pm$ 0.272
WD J101148.83+464924.17	152.9532848	46.8230704	5.681	10.8824 $\pm$ 0.5624	-23.352 $\pm$ 0.496	-70.025 $\pm$ 0.540
WD J101359.85+030553.90	153.4998209	3.0978670		20.1351 $\pm$ 0.2443	105.073 $\pm$ 0.184	-99.129 $\pm$ 0.213
WD J101401.60+030550.42	153.5071480	3.0968880	26.574	20.6894 $\pm$ 0.1936	110.107 $\pm$ 0.190	-101.150 $\pm$ 0.227
WD J101539.25–752747.50	153.9110633	-75.4634967		11.2690 $\pm$ 0.2129	-139.455 $\pm$ 0.311	-67.561 $\pm$ 0.274
WD J101539.82–752745.82	153.9134274	-75.4630451	2.684	11.5409 $\pm$ 0.4828	-140.339 $\pm$ 0.705	-71.243 $\pm$ 0.656
WD J102442.01+491351.28	156.1737922	49.2304852		12.6014 $\pm$ 0.2865	-181.958 $\pm$ 0.210	-95.849 $\pm$ 0.313
WD J102442.57+491407.82	156.1761480	49.2350740	17.423	11.5901 $\pm$ 0.4260	-182.426 $\pm$ 0.344	-96.637 $\pm$ 0.443
WD J103002.22–310135.20	157.5087674	-31.0267345		10.2653 $\pm$ 0.4845	-89.626 $\pm$ 0.339	-64.798 $\pm$ 0.474
WD J103002.31–310138.67	157.5091676	-31.0276912	3.659	10.2087 $\pm$ 0.4990	-85.395 $\pm$ 0.380	-65.254 $\pm$ 0.493
WD J112952.04–312247.21	172.4652769	-31.3788066		13.8999 $\pm$ 0.1652	-296.162 $\pm$ 0.191	219.728 $\pm$ 0.122
WD J112953.77–312243.02	172.4724986	-31.3776397	22.590	14.2005 $\pm$ 0.3007	-297.061 $\pm$ 0.341	219.713 $\pm$ 0.219
WD J122302.62–340800.00	185.7599176	-34.1339639		11.8074 $\pm$ 0.6166	-188.470 $\pm$ 0.752	-141.658 $\pm$ 0.584
WD J122302.68–340802.31	185.7601731	-34.1345908	2.382	13.4927 $\pm$ 0.7096	-186.779 $\pm$ 0.895	-138.925 $\pm$ 0.796
WD J124029.35+255948.30	190.1211382	25.9965929		10.2865 $\pm$ 0.5681	-235.037 $\pm$ 0.627	-35.049 $\pm$ 0.491
WD J124029.56+255947.81	190.1220258	25.9964738	2.904	10.2112 $\pm$ 0.4076	-233.955 $\pm$ 0.531	-32.550 $\pm$ 0.349
WD J124824.48–664037.75	192.0983149	-66.6772751		13.6669 $\pm$ 0.3154	-327.645 $\pm$ 0.259	-27.728 $\pm$ 0.305
WD J124825.45–664013.50	192.1023772	-66.6705433	24.917	14.5679 $\pm$ 0.5394	-328.029 $\pm$ 0.468	-28.199 $\pm$ 0.560
WD J124825.42+550832.61	192.1050902	55.1414257		17.0714 $\pm$ 0.2162	-107.805 $\pm$ 0.217	-217.504 $\pm$ 0.211
WD J124825.59+550830.91	192.1057717	55.1409618	2.181	16.9965 $\pm$ 0.3220	-111.970 $\pm$ 0.328	-215.297 $\pm$ 0.321
WD J132152.71–504407.04	200.4695123	-50.7351866		11.5905 $\pm$ 0.3779	-19.383 $\pm$ 0.469	23.848 $\pm$ 0.378
WD J132153.92–504354.57	200.4745356	-50.7317177	16.940	11.5753 $\pm$ 0.2937	-17.006 $\pm$ 0.355	24.615 $\pm$ 0.280
WD J133552.03+123709.07	203.9662259	12.6193339		10.0259 $\pm$ 0.0545	-123.526 $\pm$ 0.066	33.491 $\pm$ 0.043
WD J133552.15+123716.40	203.9667104	12.6213767	7.549	10.0910 $\pm$ 0.3597	-124.901 $\pm$ 0.434	34.450 $\pm$ 0.295

**Table 9** *continued*

**Table 9** (*continued*)

WD Name	R.A.	Dec.	Sep.	$\varpi$	$\mu_\alpha$	$\mu_\delta$
				(mas)	(mas yr $^{-1}$ )	(mas yr $^{-1}$ )
WD J140248.74+154433.22	210.7028894	15.7419024		11.0134 $\pm$ 0.5616	-42.396 $\pm$ 0.603	-148.719 $\pm$ 0.450
WD J140249.85+154453.37	210.7075265	15.7474894	25.743	10.6276 $\pm$ 0.6432	-42.055 $\pm$ 0.733	-149.500 $\pm$ 0.544
WD J144920.75+205419.74	222.3358875	20.9054711		13.2149 $\pm$ 0.1755	-120.029 $\pm$ 0.194	-3.471 $\pm$ 0.193
WD J144921.38+205421.86	222.3385018	20.9060554	9.040	13.3466 $\pm$ 0.2241	-123.303 $\pm$ 0.236	-3.649 $\pm$ 0.234
WD J145314.54-225858.51	223.3095891	-22.9830958		13.8344 $\pm$ 0.3679	-202.568 $\pm$ 0.434	-40.774 $\pm$ 0.423
WD J145314.72-225854.75	223.3103489	-22.9820457	4.542	14.5914 $\pm$ 0.6728	-206.104 $\pm$ 0.687	-38.284 $\pm$ 0.683
WD J145739.27+272814.87	224.4131763	27.4708850		15.0460 $\pm$ 0.1846	-92.655 $\pm$ 0.167	18.949 $\pm$ 0.183
WD J145739.77+272820.63	224.4152345	27.4724957	8.766	15.2571 $\pm$ 0.2133	-92.951 $\pm$ 0.196	22.434 $\pm$ 0.208
WD J151715.46-021902.80	229.3142711	-2.3178085		10.0298 $\pm$ 0.4878	-31.685 $\pm$ 0.505	-81.818 $\pm$ 0.419
WD J151715.49-021900.84	229.3143946	-2.3172395	2.096	10.3005 $\pm$ 0.4067	-33.610 $\pm$ 0.466	-76.820 $\pm$ 0.373
WD J152229.86-124741.75	230.6246930	-12.7948691		12.3186 $\pm$ 0.2333	61.212 $\pm$ 0.275	13.413 $\pm$ 0.204
WD J152232.31-124729.90	230.6349173	-12.7915772	37.800	12.3110 $\pm$ 0.3460	60.289 $\pm$ 0.425	13.704 $\pm$ 0.300
WD J152239.94+431306.63	230.6660700	43.2182436		10.9025 $\pm$ 0.2353	-53.525 $\pm$ 0.237	-59.453 $\pm$ 0.277
WD J152240.18+431306.13	230.6670755	43.2181088	2.682	10.9107 $\pm$ 0.2780	-57.071 $\pm$ 0.296	-58.424 $\pm$ 0.341
WD J153019.54-342353.78	232.5821497	-34.3983934		13.7398 $\pm$ 0.3004	133.588 $\pm$ 0.269	-27.817 $\pm$ 0.214
WD J153019.71-342356.51	232.5828774	-34.3991303	3.422	13.2780 $\pm$ 0.3026	136.390 $\pm$ 0.281	-22.085 $\pm$ 0.221
WD J153034.07-572421.42	232.6400901	-57.4055468		24.4933 $\pm$ 0.1103	-225.415 $\pm$ 0.110	90.537 $\pm$ 0.111
WD J153034.35-572425.84	232.6413400	-57.4067441	4.945	24.5087 $\pm$ 0.1122	-215.592 $\pm$ 0.113	97.269 $\pm$ 0.114
WD J155612.11+182907.51	239.0495810	18.4854246		11.9042 $\pm$ 0.5971	-187.152 $\pm$ 0.549	0.957 $\pm$ 0.544
WD J155612.11+182909.89	239.0496053	18.4860857	2.381	11.5064 $\pm$ 0.6388	-179.427 $\pm$ 0.566	1.689 $\pm$ 0.578
WD J155755.23-383242.75	239.4797304	-38.5458134		22.4894 $\pm$ 0.1755	-71.914 $\pm$ 0.197	-136.273 $\pm$ 0.165
WD J155755.87-383243.60	239.4824072	-38.5460503	7.585	22.2701 $\pm$ 0.1314	-69.982 $\pm$ 0.148	-136.232 $\pm$ 0.122
WD J155925.30-374421.23	239.8554544	-37.7391697		10.6021 $\pm$ 0.1033	6.161 $\pm$ 0.125	14.041 $\pm$ 0.089
WD J155925.47-374420.84	239.8561420	-37.7390513	2.003	10.4746 $\pm$ 0.3218	5.720 $\pm$ 0.394	16.134 $\pm$ 0.279
WD J155943.13+181714.22	239.9291537	18.2870074		11.9905 $\pm$ 0.2996	-117.872 $\pm$ 0.282	-63.075 $\pm$ 0.243
WD J155943.53+181716.10	239.9308003	18.2875209	5.924	12.1533 $\pm$ 0.3741	-118.682 $\pm$ 0.355	-63.816 $\pm$ 0.305
WD J164055.84+034533.83	250.2318826	3.7594146		21.6318 $\pm$ 0.1844	-175.533 $\pm$ 0.229	3.558 $\pm$ 0.175
WD J164055.96+034534.08	250.2324524	3.7594652	2.055	21.8072 $\pm$ 0.1903	-164.487 $\pm$ 0.234	-0.482 $\pm$ 0.179
WD J164837.72-353818.39	252.1571658	-35.6386258		16.7820 $\pm$ 0.0406	1.186 $\pm$ 0.054	-41.003 $\pm$ 0.041
WD J164837.72-353821.08	252.1571717	-35.6393620	2.650	16.0062 $\pm$ 0.2234	3.575 $\pm$ 0.282	-39.068 $\pm$ 0.218
WD J164853.70+494858.11	252.2233167	49.8159809		14.6919 $\pm$ 0.1851	-63.683 $\pm$ 0.211	-36.345 $\pm$ 0.268
WD J164854.12+494852.65	252.2250758	49.8144713	6.799	15.0175 $\pm$ 0.1746	-64.438 $\pm$ 0.204	-35.085 $\pm$ 0.254
WD J171937.19+013407.20	259.9044771	1.5680558		15.4507 $\pm$ 0.3276	-108.509 $\pm$ 0.273	-137.606 $\pm$ 0.198
WD J171937.68+013406.90	259.9065454	1.5679802	7.448	15.9414 $\pm$ 0.2917	-107.030 $\pm$ 0.245	-136.612 $\pm$ 0.177
WD J172603.91+323026.47	261.5158539	32.5071464		10.4958 $\pm$ 0.3264	-83.315 $\pm$ 0.354	-45.714 $\pm$ 0.453
WD J172604.97+323023.63	261.5202537	32.5063565	13.657	12.2843 $\pm$ 0.3185	-84.686 $\pm$ 0.349	-46.369 $\pm$ 0.363
WD J172830.68+072114.13	262.1274743	7.3526572		21.2759 $\pm$ 0.1506	-83.738 $\pm$ 0.144	-285.159 $\pm$ 0.114
WD J172830.82+072115.04	262.1280467	7.3528659	2.177	21.1428 $\pm$ 0.1205	-80.251 $\pm$ 0.116	-295.357 $\pm$ 0.093
WD J172929.26+291609.73	262.3711812	29.2684737		24.4408 $\pm$ 0.0464	-146.014 $\pm$ 0.047	-201.389 $\pm$ 0.053
WD J172929.64+291554.77	262.3727428	29.2643208	15.734	24.3286 $\pm$ 0.1034	-150.217 $\pm$ 0.106	-200.864 $\pm$ 0.121
WD J173423.57-220802.85	263.5981574	-22.1341407		10.3377 $\pm$ 2.0529	-6.858 $\pm$ 1.158	-3.552 $\pm$ 0.805
WD J173424.35-220807.89	263.6014344	-22.1355442	12.039	11.5769 $\pm$ 2.0196	-6.785 $\pm$ 1.877	-4.238 $\pm$ 1.037
WD J180013.41+093221.36	270.0542131	9.5386208		13.4562 $\pm$ 0.5311	-367.027 $\pm$ 0.510	-145.023 $\pm$ 0.515
WD J180014.15+093219.61	270.0572815	9.5381441	11.028	13.4576 $\pm$ 0.3541	-367.995 $\pm$ 0.347	-142.765 $\pm$ 0.336
WD J180452.09-661706.00	271.2174211	-66.2849851		12.2625 $\pm$ 0.3173	34.224 $\pm$ 0.259	3.167 $\pm$ 0.285

**Table 9** *continued*

**Table 9** (*continued*)

WD Name	R.A.	Dec.	Sep.	$\varpi$	$\mu_\alpha$	$\mu_\delta$
				(°)	(°)	(")
WD J180452.87–661709.45	271.2206909	-66.2859583	5.890	11.7501 ± 0.2487	36.597 ± 0.197	0.242 ± 0.217
WD J182518.67+553847.70	276.3265512	55.6458787		20.8992 ± 0.1391	-155.196 ± 0.157	-158.702 ± 0.165
WD J182519.30+553849.16	276.3291734	55.6462749	5.515	21.1345 ± 0.1583	-156.994 ± 0.187	-161.023 ± 0.188
WD J184905.83–545424.77	282.2736209	-54.9069843		16.4783 ± 0.0719	-87.492 ± 0.053	-23.537 ± 0.042
WD J184906.26–545424.55	282.2753901	-54.9069503	3.664	16.2976 ± 0.1955	-90.245 ± 0.142	-29.506 ± 0.113
WD J185933.28–552909.16	284.8860454	-55.4856619		15.9770 ± 0.1457	-332.412 ± 0.122	48.455 ± 0.111
WD J185934.08–552911.02	284.8893795	-55.4861625	7.036	16.0679 ± 0.2934	-336.312 ± 0.258	51.426 ± 0.224
WD J192129.72+091722.37	290.3734550	9.2893088		13.4110 ± 0.3544	-88.228 ± 0.341	-53.618 ± 0.290
WD J192129.77+091723.68	290.3736263	9.2896549	1.387	12.6388 ± 0.3536	-89.969 ± 0.324	-57.597 ± 0.276
WD J192441.31–205253.98	291.1718042	-20.8816587		11.8223 ± 0.2035	-66.810 ± 0.222	0.306 ± 0.193
WD J192442.27–205239.40	291.1758042	-20.8776067	19.845	11.6835 ± 0.3562	-67.049 ± 0.422	1.441 ± 0.348
WD J192911.25–531325.98	292.2971418	-53.2256090		18.7678 ± 0.1499	33.422 ± 0.120	-388.595 ± 0.122
WD J192912.69–531352.30	292.3031317	-53.2329200	29.315	18.3224 ± 0.1461	33.247 ± 0.113	-388.460 ± 0.108
WD J193230.35+401039.60	293.1256151	40.1767345		12.0382 ± 0.1951	-143.537 ± 0.209	-209.070 ± 0.288
WD J193231.37+401047.67	293.1298404	40.1789774	14.152	12.1740 ± 0.1987	-145.526 ± 0.219	-209.414 ± 0.257
WD J194231.45–051201.13	295.6311256	-5.2005197		10.2222 ± 0.2243	14.337 ± 0.267	-46.236 ± 0.203
WD J194231.65–051202.98	295.6319363	-5.2010312	3.441	10.2913 ± 0.4702	12.907 ± 0.569	-45.259 ± 0.434
WD J194432.04–042459.67	296.1337793	-4.4171658		10.0265 ± 0.4723	56.908 ± 0.615	-133.780 ± 0.309
WD J194432.21–042501.68	296.1344541	-4.4177335	3.169	10.4764 ± 0.5755	56.846 ± 0.780	-135.002 ± 0.395
WD J194530.33+465006.84	296.3734339	46.8334481		34.7726 ± 0.0577	-455.318 ± 0.066	-401.491 ± 0.075
WD J194530.35+465015.52	296.3735335	46.8358461	8.636	34.7116 ± 0.0509	-453.184 ± 0.060	-404.742 ± 0.066
WD J201939.74+074024.33	304.9151122	7.6732672		12.6642 ± 0.3726	-102.335 ± 0.420	-35.759 ± 0.309
WD J201940.16+074029.04	304.9168980	7.6745669	7.905	12.2056 ± 0.3094	-99.273 ± 0.360	-37.512 ± 0.279
WD J203219.82+360854.52	308.0828312	36.1482258		11.1764 ± 0.1683	42.475 ± 0.167	-55.758 ± 0.196
WD J203220.71+360847.96	308.0865251	36.1464066	12.578	10.9295 ± 0.2726	42.554 ± 0.258	-55.873 ± 0.305
WD J203801.72–343244.64	309.5072508	-34.5465006		10.0891 ± 0.3269	13.427 ± 0.349	-172.628 ± 0.256
WD J203801.84–343246.61	309.5077340	-34.5470526	2.450	11.0761 ± 0.4066	12.947 ± 0.438	-174.387 ± 0.333
WD J203834.39+491650.27	309.6427864	49.2805151		10.9860 ± 0.2307	-74.948 ± 0.262	-26.305 ± 0.297
WD J203835.87+491625.89	309.6489571	49.2737374	28.379	11.2517 ± 0.2411	-73.294 ± 0.276	-27.176 ± 0.286
WD J211534.14+324917.86	318.8935163	32.8221559		10.7101 ± 0.4716	241.086 ± 0.359	119.607 ± 0.380
WD J211534.59+324919.65	318.8953830	32.8226572	5.928	11.1115 ± 0.4195	239.708 ± 0.302	119.794 ± 0.365
WD J211723.80–415645.46	319.3522537	-41.9473075		16.8279 ± 0.2305	516.386 ± 0.220	-302.708 ± 0.204
WD J211724.10–415600.61	319.3534952	-41.9348531	44.959	16.7504 ± 0.2770	516.339 ± 0.251	-304.050 ± 0.243
WD J211812.19–520647.64	319.5508273	-52.1134726		20.0474 ± 0.1102	4.279 ± 0.090	-53.985 ± 0.090
WD J211812.39–520646.74	319.5517120	-52.1132481	2.116	20.1444 ± 0.1618	12.135 ± 0.132	-59.358 ± 0.146
WD J212436.88–301446.41	321.1542645	-30.2467007		12.6561 ± 0.5276	120.055 ± 0.551	-106.110 ± 0.487
WD J212437.00–301443.03	321.1548038	-30.2457645	3.764	12.0924 ± 0.4744	121.762 ± 0.481	-107.369 ± 0.432
WD J214538.15+110627.20	326.4097575	11.1059347		14.9158 ± 0.6026	180.090 ± 0.730	-364.789 ± 0.601
WD J214538.58+110619.69	326.4115802	11.1038357	9.928	13.8814 ± 0.4204	181.814 ± 0.540	-366.779 ± 0.424
WD J215817.63–214103.59	329.5732982	-21.6843195		12.9907 ± 0.3795	-37.834 ± 0.423	2.371 ± 0.370
WD J215817.89–214108.81	329.5743465	-21.6857653	6.276	12.9103 ± 0.3943	-39.952 ± 0.452	3.614 ± 0.394
WD J222521.42–164000.16	336.3396502	-16.6672945		11.1577 ± 0.6504	84.103 ± 0.674	-131.735 ± 0.543
WD J222522.76–164039.47	336.3452289	-16.6782316	43.823	11.1115 ± 0.6583	84.101 ± 0.746	-133.527 ± 0.562
WD J222542.67–011405.31	336.4273234	-1.2349274		13.3670 ± 0.1650	-100.930 ± 0.165	-26.960 ± 0.157
WD J222543.52–011359.51	336.4308864	-1.2333078	14.087	12.9917 ± 0.3361	-100.944 ± 0.363	-23.515 ± 0.351

**Table 9** *continued*

**Table 9** (*continued*)

WD Name	R.A.	Dec.	Sep.	$\varpi$	$\mu_\alpha$	$\mu_\delta$
	( $^\circ$ )	( $^\circ$ )	( $''$ )	(mas)	(mas yr $^{-1}$ )	(mas yr $^{-1}$ )
WD J223755.87–224712.84	339.4834022	-22.7875926		14.8839 $\pm$ 0.2004	124.775 $\pm$ 0.192	-155.773 $\pm$ 0.190
WD J223756.73–224715.01	339.4869566	-22.7882015	11.999	15.1064 $\pm$ 0.1904	124.352 $\pm$ 0.184	-157.346 $\pm$ 0.181
WD J224827.95–583031.01	342.1161408	-58.5094421		19.0166 $\pm$ 0.1092	-36.568 $\pm$ 0.088	-186.730 $\pm$ 0.124
WD J224829.50–583036.39	342.1225713	-58.5109334	13.230	19.1171 $\pm$ 0.1289	-38.476 $\pm$ 0.103	-185.783 $\pm$ 0.144
WD J230418.93–070124.51	346.0799701	-7.0244716		18.2338 $\pm$ 0.0927	240.421 $\pm$ 0.097	-224.484 $\pm$ 0.080
WD J230419.49–070149.84	346.0823042	-7.0315090	26.672	18.5819 $\pm$ 0.3101	240.012 $\pm$ 0.345	-225.269 $\pm$ 0.281
WD J230959.10+301111.01	347.4968786	30.1861831		10.8602 $\pm$ 0.3961	122.004 $\pm$ 0.311	-44.872 $\pm$ 0.329
WD J230959.14+301107.20	347.4970179	30.1851302	3.815	11.1141 $\pm$ 0.3385	119.535 $\pm$ 0.275	-46.748 $\pm$ 0.275
WD J232115.34+010211.96	350.3134624	1.0355488		16.5661 $\pm$ 0.2698	-104.998 $\pm$ 0.267	-248.714 $\pm$ 0.289
WD J232115.70+010224.59	350.3149464	1.0390470	13.679	16.3779 $\pm$ 0.2954	-104.747 $\pm$ 0.270	-251.384 $\pm$ 0.285
WD J235427.59–711909.32	358.6194068	-71.3203031		10.1262 $\pm$ 0.3332	318.796 $\pm$ 0.411	-234.997 $\pm$ 0.474
WD J235428.19–711907.67	358.6219189	-71.3198456	3.332	11.0856 $\pm$ 0.2945	319.537 $\pm$ 0.313	-234.464 $\pm$ 0.390

## REFERENCES

- Abbott, T. M. C., Adamów, M., Aguena, M., et al. 2021, *ApJS*, 255, 20, doi: [10.3847/1538-4365/ac00b3](https://doi.org/10.3847/1538-4365/ac00b3)
- Baig, S., Smart, R. L., Jones, H. R. A., et al. 2024, *MNRAS*, 533, 3784, doi: [10.1093/mnras/stae2005](https://doi.org/10.1093/mnras/stae2005)
- Becklin, E. E., & Zuckerman, B. 1988, *Nature*, 336, 656, doi: [10.1038/336656a0](https://doi.org/10.1038/336656a0)
- Bédard, A., Bergeron, P., Brassard, P., & Fontaine, G. 2020, *ApJ*, 901, 93, doi: [10.3847/1538-4357/abafbe](https://doi.org/10.3847/1538-4357/abafbe)
- Best, W. M. J., Liu, M. C., Magnier, E. A., & Dupuy, T. J. 2021, *AJ*, 161, 42, doi: [10.3847/1538-3881/abc893](https://doi.org/10.3847/1538-3881/abc893)
- Best, W. M. J., Magnier, E. A., Liu, M. C., et al. 2018, *ApJS*, 234, 1, doi: [10.3847/1538-4365/aa9982](https://doi.org/10.3847/1538-4365/aa9982)
- Beuermann, K., Dreizler, S., Hessman, F. V., et al. 2013, *A&A*, 558, A96, doi: [10.1051/0004-6361/201322241](https://doi.org/10.1051/0004-6361/201322241)
- Blouin, S., Dufour, P., Thibeault, C., & Allard, N. F. 2019, *ApJ*, 878, 63, doi: [10.3847/1538-4357/ab1f82](https://doi.org/10.3847/1538-4357/ab1f82)
- Brown, W. R., Geller, M. J., Kenyon, S. J., Kurtz, M. J., & Bromley, B. C. 2007, *ApJ*, 660, 311, doi: [10.1086/513595](https://doi.org/10.1086/513595)
- Burgasser, A. J. 2007, *ApJ*, 659, 655, doi: [10.1086/511027](https://doi.org/10.1086/511027)
- Burgasser, A. J., Geballe, T. R., Leggett, S. K., Kirkpatrick, J. D., & Golimowski, D. A. 2006, *ApJ*, 637, 1067, doi: [10.1086/498563](https://doi.org/10.1086/498563)
- Burgasser, A. J., McElwain, M. W., Kirkpatrick, J. D., et al. 2004, *AJ*, 127, 2856, doi: [10.1086/383549](https://doi.org/10.1086/383549)
- Caselden, D., Westin, Paul, I., Meisner, A., Kuchner, M., & Colin, G. 2018, WiseView: Visualizing motion and variability of faint WISE sources, *Astrophysics Source Code Library*, record ascl:1806.004
- Casewell, S. L., Debes, J., Braker, I. P., et al. 2020a, *MNRAS*, 499, 5318, doi: [10.1093/mnras/staa3184](https://doi.org/10.1093/mnras/staa3184)
- Casewell, S. L., Burleigh, M. R., Wynn, G. A., et al. 2012, *ApJL*, 759, L34, doi: [10.1088/2041-8205/759/2/L34](https://doi.org/10.1088/2041-8205/759/2/L34)
- Casewell, S. L., Braker, I. P., Parsons, S. G., et al. 2018, *MNRAS*, 476, 1405, doi: [10.1093/mnras/sty245](https://doi.org/10.1093/mnras/sty245)
- Casewell, S. L., Belardi, C., Parsons, S. G., et al. 2020b, *MNRAS*, 497, 3571, doi: [10.1093/mnras/staa1608](https://doi.org/10.1093/mnras/staa1608)
- Chambers, K. C., Magnier, E. A., Metcalfe, N., et al. 2016, arXiv e-prints, arXiv:1612.05560, doi: [10.48550/arXiv.1612.05560](https://doi.org/10.48550/arXiv.1612.05560)
- Choi, J., Dotter, A., Conroy, C., et al. 2016, *ApJ*, 823, 102, doi: [10.3847/0004-637X/823/2/102](https://doi.org/10.3847/0004-637X/823/2/102)
- Cioni, M. R. L., Clementini, G., Girardi, L., et al. 2011, *A&A*, 527, A116, doi: [10.1051/0004-6361/201016137](https://doi.org/10.1051/0004-6361/201016137)
- Cummings, J. D., Kalirai, J. S., Tremblay, P. E., Ramirez-Ruiz, E., & Choi, J. 2018, *ApJ*, 866, 21, doi: [10.3847/1538-4357/aadfd6](https://doi.org/10.3847/1538-4357/aadfd6)
- Cushing, M. C., Vacca, W. D., & Rayner, J. T. 2004, *PASP*, 116, 362, doi: [10.1086/382907](https://doi.org/10.1086/382907)
- Day-Jones, A. C., Pinfield, D. J., Ruiz, M. T., et al. 2011, *MNRAS*, 410, 705, doi: [10.1111/j.1365-2966.2010.17469.x](https://doi.org/10.1111/j.1365-2966.2010.17469.x)
- De Angeli, F., Weiler, M., Montegriffo, P., et al. 2023, *A&A*, 674, A2, doi: [10.1051/0004-6361/202243680](https://doi.org/10.1051/0004-6361/202243680)
- Deacon, N. R., & Hambly, N. C. 2007, *A&A*, 468, 163, doi: [10.1051/0004-6361:20066844](https://doi.org/10.1051/0004-6361:20066844)
- Deacon, N. R., Liu, M. C., Magnier, E. A., et al. 2014, *ApJ*, 792, 119, doi: [10.1088/0004-637X/792/2/119](https://doi.org/10.1088/0004-637X/792/2/119)
- Debes, J. H., Hoard, D. W., Wachter, S., Leisawitz, D. T., & Cohen, M. 2011, *ApJS*, 197, 38, doi: [10.1088/0067-0049/197/2/38](https://doi.org/10.1088/0067-0049/197/2/38)
- Debes, J. H., Thévenot, M., Kuchner, M. J., et al. 2019, *ApJL*, 872, L25, doi: [10.3847/2041-8213/ab0426](https://doi.org/10.3847/2041-8213/ab0426)
- Dennihy, E., Clemens, J. C., Debes, J. H., et al. 2017, *ApJ*, 849, 77, doi: [10.3847/1538-4357/aa8ef2](https://doi.org/10.3847/1538-4357/aa8ef2)
- Dey, A., Schlegel, D. J., Lang, D., et al. 2019, *AJ*, 157, 168, doi: [10.3847/1538-3881/ab089d](https://doi.org/10.3847/1538-3881/ab089d)
- Dobbie, P. D., Burleigh, M. R., Levan, A. J., et al. 2005, *MNRAS*, 357, 1049, doi: [10.1111/j.1365-2966.2005.08720.x](https://doi.org/10.1111/j.1365-2966.2005.08720.x)
- Dotter, A. 2016, *ApJS*, 222, 8, doi: [10.3847/0067-0049/222/1/8](https://doi.org/10.3847/0067-0049/222/1/8)
- Dupuy, T. J., & Kraus, A. L. 2013, *Science*, 341, 1492, doi: [10.1126/science.1241917](https://doi.org/10.1126/science.1241917)
- Dupuy, T. J., & Liu, M. C. 2012, *ApJS*, 201, 19, doi: [10.1088/0067-0049/201/2/19](https://doi.org/10.1088/0067-0049/201/2/19)
- Dye, S., Lawrence, A., Read, M. A., et al. 2018, *MNRAS*, 473, 5113, doi: [10.1093/mnras/stx2622](https://doi.org/10.1093/mnras/stx2622)
- Edge, A., Sutherland, W., Kuijken, K., et al. 2013, *The Messenger*, 154, 32
- Farihi, J., Becklin, E. E., & Zuckerman, B. 2005, *ApJS*, 161, 394, doi: [10.1086/444362](https://doi.org/10.1086/444362)
- Farihi, J., & Christopher, M. 2004, *AJ*, 128, 1868, doi: [10.1086/423919](https://doi.org/10.1086/423919)
- Farihi, J., Parsons, S. G., & Gänsicke, B. T. 2017, *Nature Astronomy*, 1, 0032, doi: [10.1038/s41550-016-0032](https://doi.org/10.1038/s41550-016-0032)
- Favieres, C. M., Kissler-Patig, M., Xu, S., & Bonsor, A. 2024, *A&A*, 688, A168, doi: [10.1051/0004-6361/202347368](https://doi.org/10.1051/0004-6361/202347368)
- Fitzpatrick, M. J., Olsen, K., Economou, F., et al. 2014, in Society of Photo-Optical Instrumentation Engineers (SPIE) Conference Series, Vol. 9149, Observatory Operations: Strategies, Processes, and Systems V, ed. A. B. Peck, C. R. Benn, & R. L. Seaman, 91491T, doi: [10.1117/12.2057445](https://doi.org/10.1117/12.2057445)
- Fontaine, G., Brassard, P., & Bergeron, P. 2001, *PASP*, 113, 409, doi: [10.1086/319535](https://doi.org/10.1086/319535)

- Fouesneau, M., Rix, H.-W., von Hippel, T., Hogg, D. W., & Tian, H. 2019, ApJ, 870, 9, doi: [10.3847/1538-4357/aaeee74](https://doi.org/10.3847/1538-4357/aaeee74)
- French, J. R., Casewell, S. L., Dupuy, T. J., et al. 2023, MNRAS, 519, 5008, doi: [10.1093/mnras/stac3807](https://doi.org/10.1093/mnras/stac3807)
- Gagné, J., Faherty, J. K., Schneider, A. C., & Meisner, A. M. 2021, CoMover: Bayesian probability of co-moving stars, Astrophysics Source Code Library, record ascl:2106.007
- Gaia Collaboration, Babusiaux, C., van Leeuwen, F., et al. 2018, A&A, 616, A10, doi: [10.1051/0004-6361/201832843](https://doi.org/10.1051/0004-6361/201832843)
- Gaia Collaboration, Brown, A. G. A., Vallenari, A., et al. 2021a, A&A, 649, A1, doi: [10.1051/0004-6361/202039657](https://doi.org/10.1051/0004-6361/202039657)
- Gaia Collaboration, Smart, R. L., Sarro, L. M., et al. 2021b, A&A, 649, A6, doi: [10.1051/0004-6361/202039498](https://doi.org/10.1051/0004-6361/202039498)
- Gálvez-Ortiz, M. C., Solano, E., Lodieu, N., & Aberasturi, M. 2017, MNRAS, 466, 2983, doi: [10.1093/mnras/stw3097](https://doi.org/10.1093/mnras/stw3097)
- Gentile Fusillo, N. P., Tremblay, P.-E., Gänsicke, B. T., et al. 2019, MNRAS, 482, 4570, doi: [10.1093/mnras/sty3016](https://doi.org/10.1093/mnras/sty3016)
- Gentile Fusillo, N. P., Tremblay, P. E., Cukanovaite, E., et al. 2021, MNRAS, 508, 3877, doi: [10.1093/mnras/stab2672](https://doi.org/10.1093/mnras/stab2672)
- Girven, J., Brinkworth, C. S., Farihi, J., et al. 2012, ApJ, 749, 154, doi: [10.1088/0004-637X/749/2/154](https://doi.org/10.1088/0004-637X/749/2/154)
- Girven, J., Gänsicke, B. T., Steeghs, D., & Koester, D. 2011, MNRAS, 417, 1210, doi: [10.1111/j.1365-2966.2011.19337.x](https://doi.org/10.1111/j.1365-2966.2011.19337.x)
- Greenstein, J. L. 1986, AJ, 92, 867, doi: [10.1086/114220](https://doi.org/10.1086/114220)
- Henry, T. J., Subasavage, J. P., Brown, M. A., et al. 2004, AJ, 128, 2460, doi: [10.1086/425052](https://doi.org/10.1086/425052)
- Heyl, J., Caiazzo, I., & Richer, H. B. 2022, ApJ, 926, 132, doi: [10.3847/1538-4357/ac45fc](https://doi.org/10.3847/1538-4357/ac45fc)
- Hoard, D. W., Debes, J. H., Wachter, S., Leisawitz, D. T., & Cohen, M. 2013, ApJ, 770, 21, doi: [10.1088/0004-637X/770/1/21](https://doi.org/10.1088/0004-637X/770/1/21)
- Hook, I. M., Jørgensen, I., Allington-Smith, J. R., et al. 2004, PASP, 116, 425, doi: [10.1086/383624](https://doi.org/10.1086/383624)
- Jalowiczor, P. A., Casewell, S., Schneider, A. C., et al. 2021, Research Notes of the American Astronomical Society, 5, 76, doi: [10.3847/2515-5172/abf49a](https://doi.org/10.3847/2515-5172/abf49a)
- Jiménez-Esteban, F. M., Torres, S., Rebassa-Mansergas, A., et al. 2023, MNRAS, 518, 5106, doi: [10.1093/mnras/stac3382](https://doi.org/10.1093/mnras/stac3382)
- Kepler, S. O., Pelisoli, I., Koester, D., et al. 2019, MNRAS, 486, 2169, doi: [10.1093/mnras/stz960](https://doi.org/10.1093/mnras/stz960)
- Kilic, M., Bergeron, P., Dame, K., et al. 2019, MNRAS, 482, 965, doi: [10.1093/mnras/sty2755](https://doi.org/10.1093/mnras/sty2755)
- Kilic, M., von Hippel, T., Leggett, S. K., & Winget, D. E. 2005, ApJL, 632, L115, doi: [10.1086/497825](https://doi.org/10.1086/497825)
- Kiman, R., Schmidt, S. J., Angus, R., et al. 2019, AJ, 157, 231, doi: [10.3847/1538-3881/ab1753](https://doi.org/10.3847/1538-3881/ab1753)
- Kiman, R., Xu, S., Faherty, J. K., et al. 2022, AJ, 164, 62, doi: [10.3847/1538-3881/ac7788](https://doi.org/10.3847/1538-3881/ac7788)
- Kiman, R., Faherty, J. K., Cruz, K. L., et al. 2021, AJ, 161, 277, doi: [10.3847/1538-3881/abf561](https://doi.org/10.3847/1538-3881/abf561)
- Kirkpatrick, J. D., Henry, T. J., & McCarthy, Donald W., J. 1991, ApJS, 77, 417, doi: [10.1086/191611](https://doi.org/10.1086/191611)
- Kirkpatrick, J. D., Reid, I. N., Liebert, J., et al. 1999, ApJ, 519, 802, doi: [10.1086/307414](https://doi.org/10.1086/307414)
- Kirkpatrick, J. D.,Looper, D. L.,Burgasser, A. J.,et al. 2010, ApJS, 190, 100, doi: [10.1088/0067-0049/190/1/100](https://doi.org/10.1088/0067-0049/190/1/100)
- Kirkpatrick, J. D., Schneider, A., Fajardo-Acosta, S., et al. 2014, ApJ, 783, 122, doi: [10.1088/0004-637X/783/2/122](https://doi.org/10.1088/0004-637X/783/2/122)
- Kirkpatrick, J. D., Kellogg, K., Schneider, A. C., et al. 2016, ApJS, 224, 36, doi: [10.3847/0067-0049/224/2/36](https://doi.org/10.3847/0067-0049/224/2/36)
- Kirkpatrick, J. D., Gelino, C. R., Faherty, J. K., et al. 2021, ApJS, 253, 7, doi: [10.3847/1538-4365/abdf107](https://doi.org/10.3847/1538-4365/abdf107)
- Kirkpatrick, J. D., Marocco, F., Gelino, C. R., et al. 2024, ApJS, 271, 55, doi: [10.3847/1538-4365/ad24e2](https://doi.org/10.3847/1538-4365/ad24e2)
- Kiwy, F., Faherty, J. K., Meisner, A., et al. 2022, AJ, 164, 3, doi: [10.3847/1538-3881/ac68e7](https://doi.org/10.3847/1538-3881/ac68e7)
- Kleinman, S. J., Harris, H. C., Eisenstein, D. J., et al. 2004, ApJ, 607, 426, doi: [10.1086/383464](https://doi.org/10.1086/383464)
- Kraft, R. P., & Luyten, W. J. 1965, ApJ, 142, 1041, doi: [10.1086/148374](https://doi.org/10.1086/148374)
- Kuchner, M. J., Faherty, J. K., Schneider, A. C., et al. 2017, ApJL, 841, L19, doi: [10.3847/2041-8213/aa7200](https://doi.org/10.3847/2041-8213/aa7200)
- Labrie, K., Anderson, K., Cárdenes, R., Simpson, C., & Turner, J. E. H. 2019, in Astronomical Society of the Pacific Conference Series, Vol. 523, Astronomical Data Analysis Software and Systems XXVII, ed. P. J. Teuben, M. W. Pound, B. A. Thomas, & E. M. Warner, 321
- Labrie, K., Simpson, C., Cardenes, R., et al. 2023, Research Notes of the American Astronomical Society, 7, 214, doi: [10.3847/2515-5172/ad0044](https://doi.org/10.3847/2515-5172/ad0044)
- Lai, S., Dennihy, E., Xu, S., et al. 2021, ApJ, 920, 156, doi: [10.3847/1538-4357/ac1354](https://doi.org/10.3847/1538-4357/ac1354)
- Lawrence, A., Warren, S. J., Almaini, O., et al. 2007, MNRAS, 379, 1599, doi: [10.1111/j.1365-2966.2007.12040.x](https://doi.org/10.1111/j.1365-2966.2007.12040.x)
- Lépine, S., & Shara, M. M. 2005, AJ, 129, 1483, doi: [10.1086/427854](https://doi.org/10.1086/427854)
- Limoges, M. M., Bergeron, P., & Lépine, S. 2015, ApJS, 219, 19, doi: [10.1088/0067-0049/219/2/19](https://doi.org/10.1088/0067-0049/219/2/19)
- Liu, M. C., Dupuy, T. J., & Allers, K. N. 2016, ApJ, 833, 96, doi: [10.3847/1538-4357/833/1/96](https://doi.org/10.3847/1538-4357/833/1/96)

- Lodieu, N., Pérez-Garrido, A., Smart, R. L., & Silvotti, R. 2019a, A&A, 628, A66, doi: [10.1051/0004-6361/201935533](https://doi.org/10.1051/0004-6361/201935533)
- Lodieu, N., Smart, R. L., Pérez-Garrido, A., & Silvotti, R. 2019b, A&A, 623, A35, doi: [10.1051/0004-6361/201834045](https://doi.org/10.1051/0004-6361/201834045)
- Looper, D. L., Kirkpatrick, J. D., Cutri, R. M., et al. 2008, ApJ, 686, 528, doi: [10.1086/591025](https://doi.org/10.1086/591025)
- Lucas, P. W., Hoare, M. G., Longmore, A., et al. 2008, MNRAS, 391, 136, doi: [10.1111/j.1365-2966.2008.13924.x](https://doi.org/10.1111/j.1365-2966.2008.13924.x)
- Luhman, K. L., Burgasser, A. J., & Bochanski, J. J. 2011, ApJL, 730, L9, doi: [10.1088/2041-8205/730/1/L9](https://doi.org/10.1088/2041-8205/730/1/L9)
- Mace, G. N., Kirkpatrick, J. D., Cushing, M. C., et al. 2013, ApJ, 777, 36, doi: [10.1088/0004-637X/777/1/36](https://doi.org/10.1088/0004-637X/777/1/36)
- Mace, G. N., Mann, A. W., Skiff, B. A., et al. 2018, ApJ, 854, 145, doi: [10.3847/1538-4357/aaa8dd](https://doi.org/10.3847/1538-4357/aaa8dd)
- Marley, M. S., Saumon, D., Visscher, C., et al. 2021, ApJ, 920, 85, doi: [10.3847/1538-4357/ac141d](https://doi.org/10.3847/1538-4357/ac141d)
- Marocco, F., Eisenhardt, P. R. M., Fowler, J. W., et al. 2021, ApJS, 253, 8, doi: [10.3847/1538-4365/abd805](https://doi.org/10.3847/1538-4365/abd805)
- Maxted, P. F. L., Napiwotzki, R., Dobbie, P. D., & Burleigh, M. R. 2006, Nature, 442, 543, doi: [10.1038/nature04987](https://doi.org/10.1038/nature04987)
- McCook, G. P., & Sion, E. M. 1999, ApJS, 121, 1, doi: [10.1086/313186](https://doi.org/10.1086/313186)
- McMahon, R. G., Banerji, M., Gonzalez, E., et al. 2013, The Messenger, 154, 35
- Meisner, A. M., Faherty, J. K., Kirkpatrick, J. D., et al. 2020, ApJ, 899, 123, doi: [10.3847/1538-4357/aba633](https://doi.org/10.3847/1538-4357/aba633)
- Minniti, D., Lucas, P. W., Emerson, J. P., et al. 2010, NewA, 15, 433, doi: [10.1016/j.newast.2009.12.002](https://doi.org/10.1016/j.newast.2009.12.002)
- Morley, C. V., Mukherjee, S., Marley, M. S., et al. 2024, ApJ, 975, 59, doi: [10.3847/1538-4357/ad71d5](https://doi.org/10.3847/1538-4357/ad71d5)
- Mumford, G. S. 1969, ApJS, 18, 429, doi: [10.1086/190195](https://doi.org/10.1086/190195)
- Nather, R. E., Robinson, E. L., & Stover, R. J. 1981, ApJ, 244, 269, doi: [10.1086/158704](https://doi.org/10.1086/158704)
- Nidever, D. L., Dey, A., Fasbender, K., et al. 2021, AJ, 161, 192, doi: [10.3847/1538-3881/abd6e1](https://doi.org/10.3847/1538-3881/abd6e1)
- Nikutta, R., Fitzpatrick, M., Scott, A., & Weaver, B. A. 2020, Astronomy and Computing, 33, 100411, doi: [10.1016/j.ascom.2020.100411](https://doi.org/10.1016/j.ascom.2020.100411)
- O'Brien, M. W., Tremblay, P. E., Klein, B. L., et al. 2024, MNRAS, 527, 8687, doi: [10.1093/mnras/stad3773](https://doi.org/10.1093/mnras/stad3773)
- Owens, D., Xu, S., Manjavacas, E., et al. 2023, AJ, 166, 5, doi: [10.3847/1538-3881/accc25](https://doi.org/10.3847/1538-3881/accc25)
- Parsons, S. G., Hermes, J. J., Marsh, T. R., et al. 2017, MNRAS, 471, 976, doi: [10.1093/mnras/stx1610](https://doi.org/10.1093/mnras/stx1610)
- Pecaut, M. J., & Mamajek, E. E. 2013, ApJS, 208, 9, doi: [10.1088/0067-0049/208/1/9](https://doi.org/10.1088/0067-0049/208/1/9)
- Qiu, D., Tian, H.-J., Wang, X.-D., et al. 2021, ApJS, 253, 58, doi: [10.3847/1538-4365/abe468](https://doi.org/10.3847/1538-4365/abe468)
- Raddi, R., Gentile Fusillo, N. P., Pala, A. F., et al. 2017, MNRAS, 472, 4173, doi: [10.1093/mnras/stx2243](https://doi.org/10.1093/mnras/stx2243)
- Ravinet, T., Reylé, C., Lagarde, N., et al. 2024, A&A, 685, A6, doi: [10.1051/0004-6361/202347954](https://doi.org/10.1051/0004-6361/202347954)
- Raymond, S. N., Szkody, P., Hawley, S. L., et al. 2003, AJ, 125, 2621, doi: [10.1086/374762](https://doi.org/10.1086/374762)
- Rayner, J. T., Toomey, D. W., Onaka, P. M., et al. 2003, PASP, 115, 362, doi: [10.1086/367745](https://doi.org/10.1086/367745)
- Rebassa-Mansergas, A., Gänsicke, B. T., Schreiber, M. R., Koester, D., & Rodríguez-Gil, P. 2010, MNRAS, 402, 620, doi: [10.1111/j.1365-2966.2009.15915.x](https://doi.org/10.1111/j.1365-2966.2009.15915.x)
- Rebassa-Mansergas, A., Solano, E., Xu, S., et al. 2019, MNRAS, 489, 3990, doi: [10.1093/mnras/stz2423](https://doi.org/10.1093/mnras/stz2423)
- Ren, J. J., Rebassa-Mansergas, A., Parsons, S. G., et al. 2018, MNRAS, 477, 4641, doi: [10.1093/mnras/sty805](https://doi.org/10.1093/mnras/sty805)
- Ren, J. J., Rebassa-Mansergas, A., Luo, A. L., et al. 2014, A&A, 570, A107, doi: [10.1051/0004-6361/201423689](https://doi.org/10.1051/0004-6361/201423689)
- Reylé, C. 2018, A&A, 619, L8, doi: [10.1051/0004-6361/201834082](https://doi.org/10.1051/0004-6361/201834082)
- Riello, M., De Angeli, F., Evans, D. W., et al. 2018, A&A, 616, A3, doi: [10.1051/0004-6361/201832712](https://doi.org/10.1051/0004-6361/201832712)
- Rodríguez-Gil, P., Gänsicke, B. T., Hagen, H. J., et al. 2005, A&A, 431, 269, doi: [10.1051/0004-6361:20042026](https://doi.org/10.1051/0004-6361:20042026)
- Rothermich, A., Faherty, J. K., Bardalez-Gagliuffi, D., et al. 2024, AJ, 167, 253, doi: [10.3847/1538-3881/ad324e](https://doi.org/10.3847/1538-3881/ad324e)
- Ruiz, M. T., Rojo, P. M., Garay, G., & Maza, J. 2001, ApJ, 552, 679, doi: [10.1086/320578](https://doi.org/10.1086/320578)
- Ruz-Mieres, D., & Zuzannakr. 2024, gaia-dpc/GaiaXPY: GaiaXPY v2.1.1, 2.1.1, Zenodo, doi: [10.5281/zenodo.11108915](https://doi.org/10.5281/zenodo.11108915)
- Salaris, M., & Bedin, L. R. 2018, MNRAS, 480, 3170, doi: [10.1093/mnras/sty2096](https://doi.org/10.1093/mnras/sty2096)
- Sanghi, A., Liu, M. C., Best, W. M. J., et al. 2023, ApJ, 959, 63, doi: [10.3847/1538-4357/acff66](https://doi.org/10.3847/1538-4357/acff66)
- Schneider, A. C., Munn, J. A., Vrba, F. J., et al. 2023, AJ, 166, 103, doi: [10.3847/1538-3881/ace9bf](https://doi.org/10.3847/1538-3881/ace9bf)
- Schlitz, G., Zuckerman, B., & Becklin, E. E. 1996, ApJ, 460, 402, doi: [10.1086/176979](https://doi.org/10.1086/176979)
- Silvestri, N. M., Hawley, S. L., West, A. A., et al. 2006, AJ, 131, 1674, doi: [10.1086/499494](https://doi.org/10.1086/499494)
- Silvestri, N. M., Lemagie, M. P., Hawley, S. L., et al. 2007, AJ, 134, 741, doi: [10.1086/519242](https://doi.org/10.1086/519242)
- Skrutskie, M. F., Cutri, R. M., Stiening, R., et al. 2006, AJ, 131, 1163, doi: [10.1086/498708](https://doi.org/10.1086/498708)
- Skrzypek, N., Warren, S. J., & Faherty, J. K. 2016, A&A, 589, A49, doi: [10.1051/0004-6361/201527359](https://doi.org/10.1051/0004-6361/201527359)
- Smart, R. L., Marocco, F., Sarro, L. M., et al. 2019, MNRAS, 485, 4423, doi: [10.1093/mnras/stz678](https://doi.org/10.1093/mnras/stz678)

- Steele, P. R., Burleigh, M. R., Dobbie, P. D., et al. 2011, *MNRAS*, 416, 2768,  
doi: [10.1111/j.1365-2966.2011.19225.x](https://doi.org/10.1111/j.1365-2966.2011.19225.x)
- Steele, P. R., Burleigh, M. R., Farihi, J., et al. 2009, *A&A*, 500, 1207, doi: [10.1051/0004-6361/200911694](https://doi.org/10.1051/0004-6361/200911694)
- Steele, P. R., Saglia, R. P., Burleigh, M. R., et al. 2013, *MNRAS*, 429, 3492, doi: [10.1093/mnras/sts620](https://doi.org/10.1093/mnras/sts620)
- Suárez, G., Vos, J. M., Metchev, S., Faherty, J. K., & Cruz, K. 2023, *ApJL*, 954, L6, doi: [10.3847/2041-8213/acec4b](https://doi.org/10.3847/2041-8213/acec4b)
- The Dark Energy Survey Collaboration. 2005, arXiv e-prints, astro, doi: [10.48550/arXiv.astro-ph/0510346](https://doi.org/10.48550/arXiv.astro-ph/0510346)
- Thorstensen, J. R., Alper, E. H., & Weil, K. E. 2016, *AJ*, 152, 226, doi: [10.3847/1538-3881/152/6/226](https://doi.org/10.3847/1538-3881/152/6/226)
- Tokovinin, A. 2022, *ApJ*, 926, 1,  
doi: [10.3847/1538-4357/ac4584](https://doi.org/10.3847/1538-4357/ac4584)
- Vacca, W. D., Cushing, M. C., & Rayner, J. T. 2003, *PASP*, 115, 389, doi: [10.1086/346193](https://doi.org/10.1086/346193)
- Vincent, O., Barstow, M. A., Jordan, S., et al. 2024, *A&A*, 682, A5, doi: [10.1051/0004-6361/202347694](https://doi.org/10.1051/0004-6361/202347694)
- Vos, J. M., Allers, K. N., & Biller, B. A. 2017, *ApJ*, 842, 78, doi: [10.3847/1538-4357/aa73cf](https://doi.org/10.3847/1538-4357/aa73cf)
- Wang, T.-g., Jiang, N., Ge, J., et al. 2019, *ApJL*, 886, L5,  
doi: [10.3847/2041-8213/ab53ed](https://doi.org/10.3847/2041-8213/ab53ed)
- Wolf, C., Onken, C. A., Luvaal, L. C., et al. 2018, *PASA*, 35, e010, doi: [10.1017/pasa.2018.5](https://doi.org/10.1017/pasa.2018.5)
- Wright, E. L., Eisenhardt, P. R. M., Mainzer, A. K., et al. 2010, *AJ*, 140, 1868, doi: [10.1088/0004-6256/140/6/1868](https://doi.org/10.1088/0004-6256/140/6/1868)
- Wu, X., Roby, T., & Ly, L. 2010, in Society of Photo-Optical Instrumentation Engineers (SPIE) Conference Series, Vol. 7737, Observatory Operations: Strategies, Processes, and Systems III, ed. D. R. Silva, A. B. Peck, & B. T. Soifer, 773716,  
doi: [10.1117/12.857728](https://doi.org/10.1117/12.857728)
- Xu, S., Lai, S., & Dennihy, E. 2020, *ApJ*, 902, 127,  
doi: [10.3847/1538-4357/abb3fc](https://doi.org/10.3847/1538-4357/abb3fc)
- Zhang, R., Liu, M. C., & Zhang, Z. 2024a, *ApJ*, 960, 105,  
doi: [10.3847/1538-4357/ad083c](https://doi.org/10.3847/1538-4357/ad083c)
- Zhang, Z., Liu, M. C., Hermes, J. J., et al. 2020, *ApJ*, 891, 171, doi: [10.3847/1538-4357/ab765c](https://doi.org/10.3847/1538-4357/ab765c)
- Zhang, Z. H., Pinfield, D. J., Day-Jones, A. C., et al. 2010, *MNRAS*, 404, 1817,  
doi: [10.1111/j.1365-2966.2010.16394.x](https://doi.org/10.1111/j.1365-2966.2010.16394.x)
- Zhang, Z. H., Raddi, R., Burgasser, A. J., et al. 2024b,  
*MNRAS*, 533, 1654, doi: [10.1093/mnras/stae1851](https://doi.org/10.1093/mnras/stae1851)
- Zuckerman, B., & Becklin, E. E. 1987, *Nature*, 330, 138,  
doi: [10.1038/330138a0](https://doi.org/10.1038/330138a0)